

The Ghost of Sagittarius and Lumps in the Halo of the Milky Way

Heidi Jo Newberg^{1,2}, Brian Yanny^{1,3}, Connie Rockosi⁴, Eva K. Grebel⁵, Hans-Walter Rix⁵, Jon Brinkmann⁶, Istvan Csabai⁷, Greg Hennessy¹⁰, Robert B. Hindsley¹⁰, Rodrigo Ibata¹¹, Zeljko Ivezić¹², Don Lamb⁴, E. Thomas Nash³, Michael Odenkirchen⁵, Heather A. Rave², D. P. Schneider¹³, J. Allyn Smith¹⁴, Andrea Stolte⁵, Donald G. York⁴

ABSTRACT

We identify new structures in the halo of the Milky Way Galaxy from positions, colors and magnitudes of five million stars detected in the Sloan Digital Sky Survey. Most of these stars are within 1.26° of the celestial equator. We present color-magnitude diagrams (CMDs) for stars in two previously discovered, tidally disrupted structures. The CMDs and turnoff colors are consistent with those of the Sagittarius dwarf galaxy, as had been predicted. In one direction, we are even able to detect a clump of red stars, similar to that of the Sagittarius dwarf, from

¹Equal first authors

²Dept. of Physics, Applied Physics and Astronomy, Rensselaer Polytechnic Institute Troy, NY 12180; heidi@rpi.edu

³Fermi National Accelerator Laboratory, P.O. Box 500, Batavia, IL 60510; yanny@fnal.gov

⁴Dept. of Astronomy and Astrophysics, University of Chicago, 5640 S. Ellis Ave., Chicago, IL 60637

⁵Max Planck Institute for Astronomy, Konigstuhl 17, D-69117 Heidelberg, Germany

⁶Apache Point Observatory, P. O. Box 59, Sunspot, NM 88349-0059

⁷Department of Physics and Complex Systems, Eotvos University, Pazmany Peter setany 1/A Budapest, H-1117, Hungary.

⁸Department of Astronomy, University of Arizona 933 N Cherry, Tucson, AZ 85726

⁹Max-Planck-Institute fur Astrophysik Karl-Schwarzschild-Str. 1 D-85741 Garching, Germany

¹⁰US Naval Observatory, Washington, D. C.

¹¹University of Strasbourg, 67000 Strasbourg, France.

¹²Princeton University Observatory, Princeton, NJ 08544.

¹³Department of Astronomy and Astrophysics, The Pennsylvania State University, University Park, PA 16802

¹⁴Department of Physics and Astronomy, University of Wyoming, P. O. Box 3905 Laramie, WY 82071

stars spread across 110 square degrees of sky. Focusing on stars with the colors of F turnoff objects, we identify at least five additional overdensities of stars.

Four of these may be pieces of the same halo structure, which would cover a region of the sky at least 40° in diameter, at a distance of 11 kpc from the Sun (18 kpc from the center of the Galaxy). The turnoff is significantly bluer than that of thick disk stars, and closer to the Galactic plane than a power law spheroid. We suggest two models to explain this new structure. One possibility is that this new structure could be a new dwarf satellite of the Milky Way, hidden in the Galactic plane, and in the process of being tidally disrupted. The other possibility is that it could be part of a disk-like distribution of stars which is metal-poor, with a scale height of approximately 2 kpc and a scale length of approximately 10 kpc.

The fifth overdensity, which is 20 kpc away, is some distance from the Sagittarius dwarf streamer orbit and is not associated with any known structure in the Galactic plane. We have tentatively identified a sixth overdensity in the halo. If this sixth structure is instead part of a smooth distribution of halo stars (the spheroid), then the spheroid must be very flattened, with axial ratio $q = 0.5$. It is likely that there are many smaller streams of stars in the Galactic halo.

Subject headings: Galaxy: structure — Galaxy: halo

1. Introduction

There is a growing body of evidence which shows that at least part of the halo of the Milky Way Galaxy was formed through the accretion of smaller satellite galaxies, and is not a relic of the initial collapse of the Milky Way. In the last decade, studies have convincingly identified moving groups and substructure in the halo by identifying groups of stars which are coherent in velocity (Majewski, Munn, and Hawley 1996; Helmi et al. 1999). Simulations have predicted the existence of many halo streamers (Lynden-Bell and Lynden-Bell 1995; Johnston, Hernquist, and Bolte 1996; Johnston et al. 1999b; Johnston, Sigurdsson, and Hernquist 1999). Most recently, studies have identified halo substructure and tidal stripping through spatial information alone (Ivezić et al. 2000; Yanny et al. 2000; Odenkirchen et al. 2001). A striking example of substructure in the halo is the identification of the Sagittarius dwarf galaxy (Ibata, Gilmore, and Irwin 1994), and its associated stream of tidally stripped stars, which appears to circle the Galaxy (Johnston, Spergel and Hernquist 1995; Ibata et al. 1997; Ibata and Lewis 1998; Johnston et al. 1999a; Helmi & White 2001; Martinez-Delgado et al. 2001).

The detection of substructure in the halo is important for our understanding of the

formation of our galaxy, and also as a test of cold dark matter (CDM) and hierarchical clustering scenarios for structure formation in the Universe. For example, Bullock, Kravtsov, and Weinberg (2001) argue that the CDM scenario generically predicts large numbers of tidally disrupted streams in the halo of the Milky Way - perhaps enough to account for the stellar halo in its entirety. They also suggest that the amount of halo substructure could distinguish among proposed solutions to the “dwarf satellite problem,” the tendency of CDM N-body simulations to predict too many satellites in the halos of galaxies like the Milky Way and M31 (Klypin et al. 1999; Moore et al. 1999).

In Yanny et al. (2000) (hereafter Paper I), we used a large sample of faint blue stars from the Sloan Digital Sky Survey (SDSS) to discover two diffuse structures of stars in the halo. Their inferred density indicated to us that these structures were disrupted remnants of a previously bound structure, such as a dwarf galaxy. We were not able to see the full extent of either structure. Ibata et al. (2001a) explained these two structures as two slices through the same great stream which completely circles the galaxy. The positions and distances of the stars in our structures exactly matched those expected from the tidal disruption of the Sagittarius dwarf spheroidal galaxy. Other pieces of this same stream have been recently reported by Dohm-Palmer et al. (2001) and a simple model of the Sagittarius breakup is given in Helmi & White (2001).

In this paper, we present additional observations of the equatorial ($-1.26^\circ < \delta_{2000} < 1.26^\circ$) data from the SDSS which probe a significantly larger angle of right ascension along the equatorial ring than in Paper I. We extend the methods of Paper I, which used faint blue stars with A-type colors to trace structure, to include the much larger sample of turnoff or near turnoff stars with F-type colors. These new data contain strong evidence for further halo substructure. The key figure in this paper is a 2D polar density histogram (RA,g) of stars with F colors (primarily F dwarf stars) shown in Figure 1 and described in detail in §5.

We expect to detect these streams of stars in addition to, or as part of, the individual stellar components of the Milky Way galaxy. Bahcall & Soneira (1984) published the “standard galaxy model,” which contained two components: a thin disk modeled with a double exponential profile with scale height 0.325 kpc, and halo modeled with a slightly squashed power law spheroid, with axial ratio 0.80. In the solar neighborhood, the spheroid stars were outnumbered by the thin disk stars by a factor of 1 in 500. Conspicuously absent was the thick disk proposed by Gilmore & Reed (1983). Since then, the popularity of models with a thick disk component has grown. The thick disk is typically modeled as a double exponential with a scale height of about 1 ± 0.5 kpc and a stellar frequency, compared with the thin disk, in the solar neighborhood of 1:10 or 1:50 (Reyle & Robin 2001; Reid & Majewski 1993; Ojha et al. 1996; Robin et al. 1996; Buser, Rong, Karaali 1999; Chen et al. 2001; Kerber,

Javiel, Santiago 2001). Stars in the thick disk component dominate the star counts 2 to 5 kpc above the plane, and have chemical and kinematic properties intermediate to the thin disk and halo populations. See Norris (1999) for a review of the status of the thick disk. See Gilmore, Wyse, & Kuijken (1989), Majewski (1993); and Wyse (1999) for reviews of Galactic components.

The literature on the subject of Galactic components is vast; studies include star count analyses, kinematics, chemical properties of stars, and comparisons with other galaxies. We have summarized only the most basic structures, which may themselves have substructure, and which some authors may break into parts or name differently. We have not discussed stellar populations in the Galactic center, such as the bulge population. See Frogel (1988), Frogel (1999) for reviews of the Galactic bulge.

2. Observations

The observations are from several time-delay and integrate (TDI) CCD scans obtained under photometric conditions in good seeing ($\text{FWHM} < 1.9''$) on twelve nights between 1998 September 19 (run 94) and 2001 February 20 (run 2126) with the Sloan Digital Sky Survey (SDSS) mosaic imaging camera (Gunn et al. 1998). See York et al. (2000) for a technical overview of the survey.

A single ‘run’ scans six 0.23 degree wide swathes of sky (‘scanlines’) separated by gaps of about 0.2 degrees. The gaps are filled by a second “strip,” containing six ‘scanlines,’ which completes a filled ‘stripe’ on the sky. The SDSS survey area is divided into 48 numbered stripes, each 2.5° wide. Each stripe follows a great circle which passes through the survey poles: $(\alpha, \delta) = (275^\circ, 0^\circ)$ and $(\alpha, \delta) = (95^\circ, 0^\circ)$. Equinox J2000 is implied throughout this paper. Most of the survey area is in the North Galactic cap. The few stripes in the South Galactic cap have separate stripe designations from their northern counterparts on the same great circle. In particular, the celestial equator ($\delta = 0$) is designated stripe 10 above the Galactic equator, and stripe 82 below. See Stoughton et al. (2001) for further details of the survey conventions.

The SDSS database contains multiple copies of many objects. We select single copies of the objects using several flags. During image processing, objects are extracted from each ‘scanline’ one ‘field’ at a time, where the breaks between fields are imposed somewhat arbitrarily every 1361 rows. So that objects which lie on these breakpoints are not lost, overlaps are processed with adjacent ‘fields.’ Objects which fall in an overlap may be in the catalog twice. Also, there are overlaps between the interleaved strips which make up

a stripe. The flag ‘OK_SCANLINE’ is assigned to only one copy of each object in an individual scanline, and uses astronomic declination limits (on the equator) to flag only the non-overlapping areas of the two strips in each stripe. If you take all objects from two interleaved runs which have ‘OK_SCANLINE’ set, you will get one instance of each object from the combined two runs. Two instances of the same object may both have ‘OK_SCANLINE’ set if they are in overlapping runs covering exactly the same part of the sky; however, since the dataset used in this paper was constructed with only non-overlapping portions of runs, selecting with the ‘OK_SCANLINE’ flag produces only one instance of each object in a given stripe. Objects can also lie on overlaps between different stripes.

The flag ‘PRIMARY’ is assigned to one copy of each object in the entire database. Each numbered stripe is assigned a region in the sky over which its objects will be ‘PRIMARY.’ Each numbered ‘run’ is assigned a region of the stripe over which it is ‘PRIMARY.’ Since the stripes overlap more toward the survey poles, the area of sky over which the stripe is ‘PRIMARY’ decreases towards its ends. The latter flag uses astronomic declination limits (on the equator) to define the non-overlapping areas of the stripes.

Most of the data used in this paper are located on stripes 10 and 82 on the celestial equator ($-1.26 < \delta < 1.26$). We also use data from stripe 11, 2.5° above the equator, stripe 12, at $\delta \sim +5^\circ$, and stripe 37, which follows part of an arc of a great circle tilted 67.5° relative to the equator. Table 1 presents details of the strips, the stripes, and the sky coverage of the data used in this paper. Not all sections of the equator scanned have both strips filled. In particular the data from the ends of runs 752, 756 and 1755 doesn’t have a corresponding filling strip. In order to have uniform star count statistics at all azimuths in these cases, double copies of the single strips were made to normalize the number counts to those areas of sky where two filled stripes were available. This is indicated by a “2” in the multiplicity column of Table 1.

The photometric system for the SDSS includes five filters, $u' g' r' i' z'$ (Fukugita et al. 1996). The system is approximately AB_ν normalized, with central wavelengths for the filters of 3543Å, 4770Å, 6231Å, 7625Å, and 9134Å, respectively, and effective widths of typically 1000Å. Since the precise calibration for the SDSS filter system is still in progress, magnitudes in this paper are quoted in the $u^* g^* r^* i^* z^*$ system, which approximates the final SDSS system (Smith et al. in preparation). These systems differ absolutely (with small color terms) by only a few percent in $g^* r^* i^* z^*$, and no more than 10% in u^* .

The data were reduced with PHOTO (Lupton et al. 2001) versions 5.1 and 5.2, and astrometrically calibrated with the ASTROM pipeline described in Pier et al. (2001).

3. Data Reduction

The SDSS software generates a database of measured object parameters and flags, including information on deblended ‘children’ of sources whose profiles overlap. One must select from this database a list of interesting objects to be used as input to analysis routines. We selected from the photometric catalog only those objects which were marked as stellar, unsaturated, and not too near the edge of the frame (too near is generally about $8''$). In order to ensure that only one instance of each object appears in the final object tables, we selected objects which were marked as “OK_SCANLINE”.

Using these criteria, we generated a catalog of 4.3 million stars to $g^* \sim 23.5$ on the equator. The total area covered is approximately 560 square degrees. Data on off-equatorial stripes add an additional 0.7 million stars over approximately 70 square degrees. Completeness vs. magnitude is discussed below, but we note here that for objects with $g^* > 22.5$, the star-galaxy separation results in most stellar objects being classified as galaxies and these thus are not prominent in our subsample.

The SDSS software measures object flux in a variety of ways. Since we are measuring stars only, we use magnitudes calculated from a fit of modeled stellar profiles (point-spread-function, or PSF, magnitudes) to each object. We correct these magnitudes for reddening using $E(B - V)$ from Schlegel, Finkbeiner, & Davis (1998), which has spatial resolution of 0.1 degrees, and the standard extinction curve (Cardelli, Clayton, & Mathis 1989), which for SDSS filters, yields: $A_{u^*} = 5.2E(B - V)$; $A_{g^*} = 3.8E(B - V)$; $A_{r^*} = 2.8E(B - V)$.

The flux of objects are presented in an inverse hyperbolic sine (asinh) representation of Lupton, Gunn, & Szalay (1999). This definition has the feature (unlike a magnitude) that it is well defined for zero or negative fluxes, which can result from measurement of no flux at the position of an object detected in a different filter. Asinh numbers and magnitudes are the same to better than 0.1% for objects with $g^* < 21$, differ by 0.1 mag at $g^* = 23.9$, and go through $g^* = 25$ at zero flux. The r^* shifts in the same way as the g^* , and thus there is negligibly little change in color due to using these asinh numbers. For the magnitude ranges of interest here ($g^* < 22.5$), the difference is unimportant. In the remainder of this paper, we will refer to asinh numbers as magnitudes.

Figure 2 shows reddening ($10 \times E(B - V)$ in magnitudes) from Schlegel, Finkbeiner, & Davis (1998) around the celestial equator. We also plot number counts in 10 degree bins for a sample of color selected stellar objects with $18 < g^* < 21.5$, $0 < u^* - g^* < 0.3$, $0.1 < g^* - r^* < 0.3$ versus right ascension around the equator. These objects, which are primarily quasars (see Figures 1, 4, and 5 of Paper I), should have a constant number density independent of Galactic latitude. Figure 2 shows that the selection of stars of similar colors and magnitudes

as a function of α around the sky is mostly unbiased. Near $\alpha = 60^\circ$, the data may be lower quality, badly calibrated, or have reddening corrections that are not well understood. For $310^\circ < \alpha < 350^\circ$, only one of two SDSS strips of data is present, and thus the counts have only half the S/N as the rest of equatorial data. The counts have been normalized upwards a factor of two and the error bars appropriately increased. Even with this normalization, it is apparent that the counts appear to fall systematically slightly below that of those at, for example, $150^\circ < \alpha < 230^\circ$. We are uncertain of the reason for this.

From inter-comparison of objects detected twice in overlapping scans, we find the rms error for stellar sources with $g^* < 19$ is typically $\sim 2\%$. For objects with $20 < g^* < 21$, typical errors are 5%, growing to 20% at $g^* = 23.5$ near the detection limit. For reference, blue stars with $0 < B - V < 0.2$ have a SDSS g^* magnitude approximately equal to their Johnson V magnitude. A theoretical color transformation is given by Fukugita et al. (1996): $g^* - r^* = 1.05(B - V) - 0.23$.

We plot in Figure 3 the rms dispersion of the difference in $g^* - r^*$ color for matched objects between two runs as a function of magnitude. For bright magnitudes this dispersion reflects the photometric errors of 2% in g and r (about $2 \times \sqrt{2} \sim 3\%$ in uncorrelated color). The photometric error increases to nearly 20% for objects near $g^* \sim 22.5$.

For some of our analyses, it is crucial to know the limiting magnitude, or more precisely the magnitude limit at which the survey can be considered complete, as a function of color and position in the sky. In the same Figure 3, we show the fraction of stars matched between two overlapping runs which make up the equatorial stripes. The matched fraction is calculated at two positions around the equator. One segment of matched data are at lower latitude, averaging $b \sim 30^\circ$ with $125^\circ < \alpha < 145^\circ$, while the other are at higher latitude with average $b \sim 50^\circ$, and $145^\circ < \alpha < 230^\circ$. Stars in three color ranges, $0.1 < g^* - r^* < 0.3$, $0.3 < g^* - r^* < 0.4$ and $0.6 < g^* - r^* < 0.7$ (all with $u^* - g^* > 0.4$) in one strip are matched to the full list of stars in the overlapping strip. The fraction which are matched is recorded as a function of g^* magnitude. Figure 3 shows that for all three color bins of the high latitude matched set, the matched fraction is constant to about $g^* \sim 22.5$, after which it drops off steeply, and somewhat more quickly for objects of bluer color.

One notes that for bright objects, the matching fraction is not 100%. This is in part due to the fact that edge overlaps were used between the interleaving stripes (so that the same exact area of sky is not sampled by each overlapping patch). Also, the reduction software doesn't resolve all objects around bright stars into separate detections. Independent matches against external catalogs indicate that the detection software detects over 99% of objects at these magnitudes ($18 < g^* < 22$).

Both segments of data at higher and lower latitudes give essentially the same results for $g^* < 22.5$. Thus any selection we do based on magnitude $g^* < 22.5$ is free of significant color or completeness bias to this limit. The variation in density of objects with quasar colors indicates there is possibly some variation in completeness limits or problems with reddening corrections at $60^\circ < \alpha < 76^\circ$ and $318^\circ < \alpha < 325^\circ$.

The imaging pipeline separates detected objects into stars and galaxies based on goodness of fit to PSFs and model galaxy profiles. For the seeing conditions under which these data were obtained, this separation produces excellent results to approximately $g^* \sim 21$. We show in Figure 4 a color magnitude image of $\approx 100,000$ objects typed as galaxies, selected around the celestial equator, and binned as a Hess diagram (Hess 1924). Nearly all galaxies have colors redder than $g^* - r^* > 0.4$, significantly redder than the turnoff stars we are interested in at $g^* - r^* \sim 0.3$. There is some leakage of stars into the galaxy population for $g^* - r^* \sim 0.3$ at $g^* > 22.5$, again below the limits set by Figure 3. The galaxy population’s localization in color-magnitude space affects none of the conclusions made here about turnoff-color star counts.

4. The Ghost of Sagittarius

Since the positions and colors of the giant branches and horizontal branches of dwarf galaxy companions to the Milky Way differ considerably as a function of the dwarf’s metallicity, age and stellar population mix, these features can be used as identifying signatures of a given dwarf galaxy or cluster. In this section, we explore the color-magnitude distribution of stars in previously detected clumps. This discussion will motivate our use of F-colored stars to detect spatial structure in the next section.

Using a technique similar to that of Majewski et al. (1999), we will construct a color-magnitude diagram of the two concentrations of stars from Paper I. To avoid confusion in referencing overdensities of stars, we will name them by the named triple $Sl \pm b - g$ where $(l \pm b)$ are the Galactic coordinates of the approximate center of the structure (where it intersects a SDSS stripe), and g is the approximate g^* magnitude of the ‘turnoff’ F dwarf stars in that structure. If the structure is identified with a known halo component, such as the Sagittarius dwarf, then the identification may appear in parentheses after the structure name. Under this naming convention, the two structures identified in Paper I are given the names S341+57–22.5 and S167–54–21.5.

For structure S341+57–22.5, we used stars marked as ‘PRIMARY’ in stripes 10 and 11 with $200^\circ < \alpha < 225^\circ$ and $u^* - g^* > 0.5$. The cut in $u^* - g^*$ eliminates blue quasars

which would otherwise dominate the faint blue edge of the color-magnitude diagram. The ‘PRIMARY’ stars come from non-intersecting portions of stripes. Since the stripes are parts of great circle arcs, the non-overlapping portion of the stripe is thinner towards the survey poles than it is on the survey equator. On the celestial equator at $\alpha = 200^\circ$, the width of stripe 10 and 11 together is 4.8 degrees. On the celestial equator at $\alpha = 225^\circ$, the width of the two stripes is 3.8 degrees. The total area covered is 110 square degrees.

Due to the large number of stars in this area of sky, we generated an image of counts-in-cells of the color-magnitude diagram, with a bin width of 0.02 in $g^* - r^*$ and 0.05 in g^* . In order to reduce the number of field stars in the image, we subtracted a similarly generated color-magnitude image of stars in a similar portion of the sky which does not contain the Sagittarius dwarf. The subtracted stars are from stripe 10 and 11, $170^\circ < \alpha < 180^\circ$, plus twice stripe 10, $230^\circ < \alpha < 235^\circ$ (SDSS has not yet processed data in the $230^\circ < \alpha < 235^\circ$ range for stripe 11).

For stars at S341+57–22.5, the resulting Hess color-magnitude diagram image (with a greyscale stretch proportional to the square root of the number of stars in each bin) is shown in Figure 5. One can clearly see the turnoff at $(g^* - r^*, g^*) = (0.2, 22.5)$, the giant branch at $(g^* - r^*, g^*) = (0.5, 22)$ running to $(g^* - r^*, g^*) = (0.6, 20.5)$, blue stragglers at $(g^* - r^*, g^*) = (-0.1, 21.5)$, a blue horizontal branch at $(g^* - r^*, g^*) = (-0.15, 19.2)$ and a clump of red stars at $(g^* - r^*, g^*) = (0.55, 19.6)$. For comparison, we show in Figure 6 the identical plot for the Sagittarius dwarf itself, with data from Marconi et al. (1998). Since this Sagittarius dwarf data were taken with V and I filters, and the dwarf is much closer than the dispersed clump (23 vs. 45 kpc), we arbitrarily aligned the clump of red stars and applied a linear correction in the color direction so that the distance between the clump of red stars and the point where the horizontal branch and the main sequence meet is the same in each image. The adopted transformation equations are: $g^* = V + 1.39$ and $(g^* - r^*) = 0.9(V - I) - 0.41$. The relation between g^* and V includes both the difference in distance modulus and the filter transformation. Any differences in reddening or errors in reddening correction for either data set are implicitly included in the transformation. The adopted transformations are very similar to the relations derived the theoretical filter curves as given in Fukugita et al. (1996).

The similarity of color-magnitude diagrams can be judged from the color of the turnoff, the distance from the horizontal branch to the turnoff, the slope and degree of population of the red giant branch, the presence or absence of blue stragglers, and the color distribution of stars along the horizontal branch. Though there are some differences (most notably - the Sagittarius dwarf photometry shows few if any blue horizontal branch stars), the agreement between the color magnitude diagrams for the Sagittarius dwarf and our 110 square degree

patch of sky on the equator is striking, and leaves little doubt that the tidally disrupted clumps of stars discovered in Ivezić et al. (2000) and Paper I are in fact pieces of the Sagittarius dwarf stream, in exactly the positions predicted by Ibata et al. (2001b).

It is interesting to estimate the fraction of the Sagittarius dwarf which is present in our observed piece of its orbit. One measure is the number counts of the clump of red stars. We estimate that there are 500 ± 50 clump of red stars in the 110 square degree patch of sky with $19.30 < g^* < 19.65$ and $0.52 < g^* - r^* < 0.66$. For this estimate, we measured the clump of red in the unsubtracted color-magnitude image to reduce the statistical noise in the measurement (the background was determined by linear interpolation). Ibata, Gilmore, and Irwin (1995) find 17,000 horizontal branch stars in a patch of sky thought to contain half the mass of the Sagittarius dwarf. We detected about $500/34,000 = 1.5\%$ as many red stars in the clump as are present in the dwarf itself in a portion of its orbit extending 4.4° on the sky. The orbit is roughly perpendicular to our scan line and presumably extends over 360° on the sky. If the stellar density along the stream were constant (admittedly a naive assumption), and the stream wraps around on itself (so as not to produce multiple wraps at different positions), then this implies about as many stars (1.2 times as many in this calculation) in the stream as in the undisrupted dwarf. This number is interesting, but quite unreliable as the fraction of stars in the clump of red stars could easily differ between or within the dwarf and the stream.

Using exactly the same procedure as for S341+57–22.5 (Sagittarius), we generate a color-magnitude image for S200–24–19.8, which has also been tentatively identified as a piece of the Sagittarius stream by Ibata et al. (2001a). Since we have no data adjacent to stripe 82, we used the full width of the collected data (there is no change in the δ -width of the stripe on the sky as a function of right ascension). We used all stars with $15^\circ < \alpha < 50^\circ$ to make the clump color-magnitude image. We then subtracted a color-magnitude image of all stars with $10^\circ < \alpha < 15^\circ$ plus double-counting all of the stars with $0^\circ < \alpha < 5^\circ$ and $50^\circ < \alpha < 55^\circ$. The resulting color-magnitude image is shown in Figure 7. One can see a clear turnoff, a giant branch, and blue straggler stars. The horizontal branch and clump of red stars, though possibly faintly present, are not compelling. There are definitely blue horizontal branch stars present, since this clump was originally detected in A-colored stars in Paper I. The number of blue horizontal branch stars in the Sagittarius south stream is only a third the number in the northern stream. This color-magnitude diagram is consistent with that of the Sagittarius dwarf, but does not present as compelling an identification as that in the north.

5. Halo structure in F stars

5.1. Distribution on the celestial equator

Our detection of halo structure in Paper I relied on the standard candle characteristics of A-colored blue horizontal branch stars. The results of the previous section demonstrate our ability to examine the structure of the Milky Way using stars as faint as F dwarfs. If it is possible to use the much larger numbers of these main sequence stars, one anticipates that much more tenuous halo structures could be discerned, though not as far out into the halo. We pursue such a path.

From stripes 10 and 82, we generate a catalog of 4,270,645 stars with $u^* - g^* > 0.4$ and $-1.0 < g^* - r^* < 2.5$. The $g^* - r^*$ color range is wide enough to include essentially all stars. In this section, we will be using not just the ‘PRIMARY’ stars, but all of the unique stars from the runs used to fill in stripes 10 and 82 as detailed in Table 1. This way, the width of the stripe in declination does not change as a function of right ascension. The $u^* - g^*$ color cut removes primarily low redshift QSOs.

In Figure 8 we show a color-magnitude image of all of the stars centered in the direction $(l,b) = (5,40)$, $230^\circ < \alpha < 240^\circ$ in stripe 10. The stars with $g^* - r^* \sim 0.5$ and $g^* \sim 18$ are thought to be associated with the thick disk of the Milky Way. The stars with $g^* - r^* \sim 1.3$ are M stars in the thin disk, the thick disk, and, at $g^* > 22$, the halo. The bluer stars ($g^* - r^* \sim 0.3$) are generally ascribed to the halo. The clear separation in turnoff color between the “thick disk” and “halo” was described by Chen et al. (2001). The stars we are interested in are the bluer stars with $g^* - r^* \sim 0.3$, at $g^* > 19$, which are associated with the halo population.

To separate the thick disk stars from halo stars, we select 334,066 stars in stripes 10 and 82 (which are both on the celestial equator) with $0.1 < g^* - r^* < 0.3$, keeping the $u^* - g^* > 0.4$ color cut. This cut includes only the bluer “halo” stars; we have so many stars that we have the luxury of throwing half of them away to reduce thick disk contamination and keep a much smaller range of dwarf star absolute magnitudes in the sample. We plot this sample of stars in a 2D polar density histogram in Figure 1. This figure is similar to the wedge plots of Paper I (see Figure 3 of that paper), but is displayed in an image by binning all the stars that would have appeared as individual dots within each pixel of the image. The Sun is located at the center of the plot. Stars of the same apparent magnitude are at the same radial distance from the center of the plot, with $g^* = 11$ at the center of the plot and $g^* = 24$ at the edge (though the data cuts off at $g^* = 23.5$). If each star has the same intrinsic magnitude (roughly the magnitude of an F main sequence star), then the radius from the center of the diagram scales as the logarithm of the distance from us. Typical

distances probed with turnoff stars range from a few kpc to about 60 kpc at the edge of the plot ($g^* = 23$).

The shading of each box indicates the relative number of F stars within the pixel’s azimuth and magnitude ranges, with 7.69 pixels/magnitude. It is generated by calculating for each star in the sample the (x, y) position the star should go on the paper, and then assigning it to the pixel which covers that spot.

Figure 1 does not show the smooth distribution of stars expected from a power law spheroid or exponential disk stellar density distribution. The overdensities of stars at $(\alpha, g^*) = (210^\circ, 22)$ and $(\alpha, g^*) = (40^\circ, 21)$ are F dwarfs associated with S341+57–22.5 and S167–54–21.5 (Sagittarius). The dark line at $\alpha = 229^\circ$ is the main sequence turnoff of the globular cluster Pal 5.

The feature at $\alpha = 60^\circ$ is exactly coincident with a large interstellar dust cloud at that position in the sky, and does not represent halo structure. When the reddening correction is that large, one must worry about the distance to the source(s) of reddening, and the accuracy of the maps. Small differences in applied reddening change the intrinsic colors of the selected objects. The counts in this direction are consistent with over-correction for reddening, which moves redder stars into the color selection box. As is apparent in the color-magnitude hess diagrams, the redder turnoff stars are more prevalent at brighter magnitudes.

Locations of other interesting overdensities are labeled in Figure 1 and summarized in Table 2. These and other overdensities will be discussed in detail below.

5.2. Spheroid models

What do typical Galactic stellar component models, such as an exponential thick disk or a power law spheroid, look like in a wedge image such as that of Figure 1? We will use the term ‘spheroid’ to describe any smooth distribution of stars in the halo of the Milky Way, regardless of its density profile (in addition to the known thin and thick disk populations). The halo of the Milky Way is a region of space containing gravitationally bound matter. The the halo stars of the Milky Way are a combination of dwarf galaxies, globular clusters, streamers, a smooth component (spheroid). The usual density profile for the Galactic spheroid is a power law, or alternatively a flattened power law with mass flattening parameter q , given by:

$$\rho = \rho_o(X^2 + Y^2 + Z^2/q^2)^{\alpha/2},$$

where X , Y , and Z are the usual Galactocentric coordinates with Z perpendicular to the Galactic plane, and ρ_o sets the density scale. If $q = 1$, the model is spherically symmetric. α is thought to be about -3.2 ± 0.3 (see Paper I).

To generate the wedge image, we must transform to a heliocentric coordinate system, (l, b, R) , where R is the distance from the Sun. In this coordinate system, the number of stars per magnitude bin is given by:

$$\frac{dN}{dm} = \frac{dR}{dm} \frac{dN}{dR} = \left(\frac{R}{5}\right)(\Omega R^2 \rho_o r^\alpha),$$

where

$$r^2 = R_o^2 + QR^2 - 2R_oR \cos(l) \cos(b),$$

$$Q = \cos^2(b) + \sin^2(b)/q^2.$$

In our simulations, we assume the distance to the center of the galaxy, R_o , is 8.0 kpc. In our plots, the number of pixels in a given apparent magnitude annulus of width dm is proportional to $(m - 11)$, and the width of the data in declination is constant. Therefore,

$$\Omega \propto (m - 11)^{-1},$$

as dm is approximately constant for each pixel in the wedge image. In this way we correct for the angular size of each pixel.

In order to make the simulation, we need to relate the distance R to the apparent magnitude m . For this we need to know the approximate absolute magnitude of the stars in Figure 1. Clearly, there will be a spread in stellar magnitudes, which should result in a broader distribution in the data than in the simulated image. We find an estimate of the magnitudes of turnoff stars by using the distance in magnitudes from the horizontal branch of the S200–24–19.8 (Sagittarius, from Paper I) to the turnoff of the Sagittarius stars in the Figure 1, stripe 82. Figure 9 shows the distribution of apparent magnitudes for stars with $30^\circ < \alpha < 45^\circ$. In each magnitude bin, we have subtracted the number of stars in a similar region of the equator that does not include the Sagittarius stream ($20^\circ < \alpha < 25^\circ$ and $45^\circ < \alpha < 55^\circ$). The range of apparent magnitudes at the peak of the distribution is $21.1 < g^* < 21.8$. Assuming a horizontal branch absolute magnitude $M_{g^*} \sim 0.7$ and $g^* = 18$ (Paper I), the absolute magnitudes of the stars in the image are estimated to be in the $3.8 < M_{g^*} < 4.5$ range, quite typical for F dwarfs. We adopt $M_{g^*} = 4.2$ as the typical magnitude of a turnoff star.

We would like to draw your attention to some special azimuthal directions on the wedge plot of Figure 1. The Galactic plane intersects the plane of the plot at $\alpha = 103^\circ$, and goes

straight through the plot center to $\alpha = 283^\circ$. The place where $l = 0^\circ$ is at $\alpha = 228^\circ$, almost in the direction of Pal 5 at $\alpha = 229^\circ$. In the celestial equatorial plane, this is not the direction of the Galactic center, but above the Galactic center in the direction which will intersect the Z-axis of the Galaxy. If the Galactic spheroid were very prolate ($q \rightarrow \infty$), then the highest density of stars intersected by the celestial equator would be at $l = 0^\circ$. If the spheroid were flattened into a pancake ($q \rightarrow 0$), the highest density of stars would be in the Galactic plane at $\alpha = 283^\circ$ ($b = 0^\circ, l = 32^\circ$), and there would be another high density of stars at $\alpha = 103^\circ$ ($b = 0^\circ, l = 212^\circ$); the relative densities would depend on how quickly the power law drops off. If the spheroid is spherical, the highest density will be in the direction of the closest approach to the center of the Galaxy. This direction does not depend on the slope of the power law or the inferred absolute magnitude of the stars. We show in Figures 10a, 10b, and 10c the wedge images which result from $q = 0.5, 1.0$, and 1.5 power law spheroids with $\alpha = -3.5$.

Using a similar procedure to that for the spheroidal models, we can generate a simulated exponential disk as seen in the cross section of the celestial equator. The relevant equations for the disk density profile models are:

$$\rho = \rho_o e^{-r/s_l} e^{-|Z|/s_h},$$

$$\frac{dN}{dm} = \frac{dR}{dm} \frac{dN}{dR} = \left(\frac{R}{5}\right) (\Omega R^2 \rho_o e^{-r/s_l} e^{-|Z|/s_h}),$$

where $r^2 \equiv X^2 + Y^2$ and X, Y, Z are standard Galactocentric coordinates with the Sun at (X,Y,Z) = (-8.0,0,0). Ω is the same as in the spheroid model. A simulated exponential disk with scale length $s_l = 3$ kpc and scale height $s_h = 1$ kpc is shown in Figure 10d. We used the same absolute magnitude for the simulated stars. Exponential disks generally put concentrations of stars at $b = 0$ ($s_h \ll s_l$). They can put concentrations of stars at $l = 0$, if $s_h \gg s_l$.

5.3. Overdensity at $\alpha = 190^\circ$ - S297+63–20.0

Armed with these results, we turn our attention again to the data in the wedge plot of Figure 1. Neither an exponential disk model nor a power-law model can put a density peak at $180^\circ < \alpha < 195^\circ$, where $(l, b) = (280^\circ, 60^\circ)$. We tentatively identify the concentration at about $g^* = 20.5$ in Figure 1 as a stream or other diffuse concentration of stars in the halo, and name it S297+63–20.0). Figure 11 shows the color-magnitude diagram for stars with $180^\circ < \alpha < 195^\circ$.

A recent paper by Vivas et al. (2001) present corroborating evidence for this stream

from observations of 5 clumped RR Lyraes at $\alpha = 197^\circ$, at a similar inferred distance from the Sun (20 kpc).

5.4. Overdensity near $\alpha = 125^\circ$ - S223+20–19.4

We now turn our attention to the concentration of stars near $\alpha = 125^\circ$ at $g^* \sim 19.5$. As we noted above, it is possible to put concentrations of stars near the Galactic plane near the anti-center ($l \sim 180^\circ$) with either an exponential disk or a flattened spheroidal power law model ($q < 0.6$). These stars are too faint to be produced by thin disk or thick disk stars from the double exponential profiles of any standard models. As we will show in §5.7, it would be necessary to postulate an unusually flattened power law distribution, or an unusually large scale length exponential disk distribution, to put enough stars this far away from the Galactic center and still fit the number counts towards the Galactic center.

A color-magnitude image for stars in this direction is shown in Figure 12. Most of the brighter, bluer stars ($g^* < 18.5$, $0.4 < g^* - r^* < 0.6$), presumably thick and thin disk, are part of a distribution with a redder turnoff than the fainter stars at ($g^* > 20$). What is stunning about the color-magnitude image in this direction is that the fainter, bluer stars appear to follow a main sequence, as if the stars are all at about the same distance from the Sun. In any kind of exponential disk or power law distribution, one expects a much broader distribution of distances, which spreads the stars in the vertical direction on the color-magnitude diagram. See Figure 6a of Layden & Sarajedini (2000) for an example of how a dwarf spheroidal in the field looks in such a CMD.

We show the shallow depth of the structure quantitatively in Figure 13. Figure 13(a) shows power law models for a variety of slopes and flattenings in the direction $(\alpha, \delta) = (125^\circ, 0^\circ)$. Figure 13(b) shows a variety of exponential disks in the same direction. Compare the widths of the peaks of these models with the width (in magnitude) of the main sequence at $\alpha \sim 125^\circ$ shown in Figure 13(c). The black line gives star counts vs. magnitude in the color range $0.1 < g^* - r^* < 0.3$. Note the peak centered at $g^* = 19.4$. If the data were broader than the model, we might expect that the data represented stars with a range of absolute magnitudes. Since the data are narrower than all of the models, no power law or exponential disk model is a good fit to the data. The spheroid models are all very poor fits to the data. The only exponential model with any hope of fitting the data has a scale height of 2 kpc and a scale length of 10 kpc. Even this model produces a peak which is a little wide for comfort.

The red line in Figure 13(c) shows the magnitude distribution of all stars with $117^\circ <$

$\alpha < 130^\circ$, $u^* - g^* > 0.4$, and $0.44 < g^* - r^* < 0.48$. The peak in this plot is fainter, since at the redder colors the stars are intrinsically fainter. The peak is narrower because these stars are on the main sequence rather than at the turnoff, where there is a broader range of intrinsic brightnesses of stars. The actual width of the stellar group must correspond to significantly less than one magnitude in distance modulus. Figure 13(c) also shows a sample model counts of a dwarf spheroidal galaxy at the distance of the stellar excess, offset from the Galactic center, at $(l, b, R_{GC}) = (212^\circ, 0^\circ, 18\text{kpc})$. The fact that is model nominally fits the SDSS stars counts allows the possibility of a newly discovered dwarf galaxy in the Galactic plane, though this is not the only possible interpretation (see §5.7).

One also verifies that incompleteness at the faint end as a function of color is not responsible for the turnoff-like feature in Figure 12. The tests of §3 indicate that this is not the case for stars with $g^* < 22$, well below the turnoff and main sequence seen here at $19.4 < g^* < 21.5$. We adopt the name S223+20–19.4 for this structure.

5.5. Overdensity near $\alpha = 75^\circ$ - S200–24+19.8

Now we look at stars at $\alpha = 75^\circ$ in Figure 1 and see if those stars can be explained by smooth components. See Figure 14 for evidence that the excess on this side of the plane is also thinner than expected for a power law or exponential disk model. For this figure, we tightened up the color range plotted, to reduce contamination from the thick disk. As was evident in Figure 2, the data in this region are of lower quality. In §5.9, we will show that the measured thick disk turnoff is much redder in this data, and may indicate a calibration error or incorrect reddening correction applied here. Although the absolute photometry is suspect in this region, we still detect an unexpectedly tight magnitude peak at $g \sim 19.8$. Figure 15 shows a CMD of stars in stripe 82, $70^\circ < \alpha < 77^\circ$. This structure is named S200–24–19.8.

5.6. Other SDSS data near the Galactic plane - S218+22–19.5, S183+22–19.4

We looked through other SDSS data sets to see if the excess of stars near the plane showed up in other runs. We have data at low Galactic latitude in stripes 12 and 37. Figure 16 shows wedge plots for the ends of stripe 12 and 37. These data include 153,286 stars of all colors in stripe 12 with $122^\circ < \alpha < 135^\circ$ and 252,099 stars in stripe 37 with $112 < \alpha < 125^\circ$. Figure 16 shows wedge plots for the ends of stripe 12 and 37.

The large increase in stars near the Galactic plane at Galactic latitude about $+20^\circ$ and $g^* \sim 19.5$ is apparent in stripes 12 and 37 as well. The magnitudes of the stars near the

ends of stripe 12 and 37 is similarly as narrow, and peaked at a similar magnitude, as those at the end of stripe 10. We adopt the labels S218+22–19.5 and S183+22–19.4 for these apparent overdensities.

Figure 17 shows a CMD of stars in stripe 37, separated by 40 degrees on the sky from those of Fig 12 in Galactic longitude (at about the same $b = +20$). The similarity between Figure 17 and Figure 12 is remarkable. The color-magnitude diagram for S218+22–19.5 looks the same as well.

5.7. Fits to the Galactic spheroid

Now that we have identified several large features in the data which are not consistent with a smooth distribution of stars, we will attempt to constrain spheroid models. In Figure 18, we show the distribution in magnitude for stars with $0.1 < g^* - r^* < 0.3$, $u^* - g^* < 0.4$, and $230^\circ < \alpha < 240^\circ$. We would be very surprised if these stars were not consistent with a spheroid population. The figure shows a very broad distribution in magnitudes, most consistent with a flattened ($q \sim 0.5$) power law with slope of $\alpha \sim -3$, though one could imagine fitting other power law distributions. Notice that the magnitude distribution in this direction is not consistent with an exponential disk with large scale lengths, especially for $g^* > 20$.

We selected all of the stars with $u^* - g^* > 0.4$, $19.0 < g^* < 20.0$, and $0.1 < g^* - r^* < 0.3$. The number of these stars as a function of right ascension is shown in black in Figure 19. We then attempted to fit spheroid models (also shown in Figure 19) to the data. We don't expect many thick disk stars in this plot, since we have selected only stars bluer than the nominal turnoff. We expect very few thin disk stars at these faint magnitudes. The models are generated by integrating the models of §5.2 over our apparent magnitude range, $19 < g^* < 20$. With only angular information, there is very little difference between models with different power law slopes or different assumed absolute magnitudes for the stars. There is greater sensitivity to the flattening of the spheroid. The only way to fit the star counts on both sides of $\alpha = 280^\circ$ is with a very large flattening, such as $q = 0.5$. More spherical models can fit the slope near $\alpha = 250^\circ$, but do not put enough stars at $\alpha = 320^\circ$. Note that we did not attempt to fit a triaxial halo, which has been used by other authors (Larsen & Humphreys 1996) to explain an interesting asymmetry in the blue star counts around the Galactic center.

As a class, the power law models cannot put enough stars around $\alpha \sim 100^\circ$ to explain the high counts there. We already encountered difficulty fitting this feature with a power

law in Figures 13 and 14, but it is good to see the discrepancy in this plot as well. In order to produce anything close, one would need a flattening more like $q = 0.2$, which is quite a bit lower than anyone has previously considered and still doesn't fit well.

Since a power law spheroid does not seem a good fit to these stars, we look to other proposed Galactic components to fit the data. Evidence for a metal weak thick disk has been given by Morrison, Flynn, & Freeman (1990), and Norris (1994). Chiba & Beers (2000), using kinematics of faint blue stars, find a scale length for this component of 4.5 kpc. An exponential disk with a scale height of 2 kpc and a scale length of 10 kpc produces our best fit to the angular data near the Galactic plane. We need the large scale length to put enough stars out at $\alpha \sim 100^\circ$. This model gives a surprisingly good fit to the data. It is important to remember that the stars fit here are not the ones routinely assigned to the thick disk; they have a bluer turnoff. This would imply that we are seeing an ‘even-thicker-disk’ of different metallicity (or age) from the ‘thick disk.’ The only data that this model contradicts is the fainter star counts in Figure 18. It does not explain the narrow magnitude profiles in Figures 13 and 14. The center of the peak near the anticenter is slightly shifted between the exponential disk model and the data. This shift cannot be reduced by small changes in the scale lengths, assumed stellar absolute magnitudes, or the Sun’s distance from the Galactic center. It could be reduced by moving the Sun to 0.2 kpc above the Galactic plane (or by lowering the exponential disk model below the plane of the thin disk by a similar amount). We placed the Sun 20 pc above the Galactic plane in our standard model, in keeping with recent estimates of this parameter (Hammersley, et al. 1995; Cohen 1995; Binney, Gerhard, & Spergel 1997; Humphreys & Larsen 1995; Mendez & van Altena 1998; Chen et al. 2001).

We have proposed two possible explanations for the overdensity S223+20-19.4. The first possibility is that it is a previously undiscovered dwarf galaxy (probably in the process of tidally disrupting), or a stream from a dwarf galaxy. The other is that it is part of a smooth, metal-poor Galactic component with a double exponential profile with about 2 kpc scale height and 10 kpc scale length. One cannot produce this many star counts near the Galactic anticenter with a power law distribution of stars. We do not expect stars with these blue colors in the thick disk. We will now show that the star counts do not fit exponential density models with the previously measured scale heights and scale lengths of the thin and thick disks.

There are two issues that were not addressed in the previous model fits in Figure 19. We did not consider that the metallicity of the thick disk could have changed as a function of scale height. We also did not use our knowledge of the local normalization of stars from the various Galactic components to check whether the stellar distributions could be reasonably attributed to a known and measured disk component.

To address these issues, we selected all of the stars in a broader color range ($0.2 < g^* - r^* < 0.5$) and in five magnitude ranges: $15.5 < g^* < 16.5$, $16.5 < g^* < 17.5$, $17.5 < g^* < 18.5$, $18.5 < g^* < 19.5$, and $19.5 < g^* < 20.0$. This should contain nearly all turnoff stars in the thick disk and halo populations, and at the bright end the older turnoff stars in the thin disk. The densities of these distributions as a function of right ascension are shown in Figure 20. We can now fit models to these data plots as a set. Since the stars are redder than in the previous plot, we assume they are fainter, using $M_{g^*} \sim 5.0$, which is about the absolute magnitude of the Sun. First, we fit the standard thin disk (scale height 0.25 kpc and scale length 2.5 kpc) and thick disk (scale height 1.0 kpc and scale length 3.0 kpc, with a local ratio of turnoff stars of 1:30 of the thin disk stars). The models are fit to the data at only one point. They are forced to match the data at $\alpha = 240$ for stars near $g^* = 17$. This fit sets the number of stars in this color range in the thick disk in the solar neighborhood to a reasonable value.

The star counts for standard thin and thick disk models do not fit. The discrepancy is most pronounced for the fainter star counts, where we see too many stars near the Galactic center and too few stars near the anticenter. We cannot move stars from the center to the anticenter by tweaking the assumed absolute magnitudes of the stars, the distance from the Sun to the center of the Galaxy, or the ratio of thin disk to thick disk stars. As we have seen, adding a power law component will also not help add star counts near the anticenter. As we saw in Figure 19, the way to significantly increase the number of stars at faint magnitudes is to add a component with larger scale height and scale length.

We could take the thin disk and thick disk models and add an additional exponential disk model to attempt to fit the data. Since we now have so many adjustable parameters, we decided to fit only a ‘thin disk’ and an ‘metal-weak thick disk (MWTD),’ and were able to fit the data about as well. We used a thin disk with a scale height of 300 pc and a scale length of 2.8 kpc, and a MWTD with a scale height of 1.8 kpc, a scale length of 8 kpc, and a thin disk to MWTH ratio of 100:1 in the solar neighborhood (for stars of this color range). We also used separate assumed absolute magnitudes for the two components: $g^* = 5.0$ for the thin disk and $g^* = 4.2$ for the MWTD. This seemed reasonable since the color-magnitude plots show that the apparently fainter stars are bluer than the apparently brighter stars in our samples. However, the results are fairly insensitive to our assumed absolute magnitudes. Figure 20 shows the model in red, with the thin disk and MWTD components in green and blue, respectively. With this model, the brighter star counts are dominated by the thin disk, and the fainter star counts are dominated by the MWTD.

We do not claim to show from this demonstration that a thick disk is ruled out. We have done the exercise of adding the third, thick disk exponential to the model, and it makes little

difference. If we adjust slightly all of the parameters, a thick disk with reasonable properties can be easily added to the model. We refrain from quoting numbers for this, since there are so many correlated parameters in this model that the individual values of each parameter may have little meaning. The thick disk may help adjust the relative numbers of redder and bluer turnoff stars in detail. For example, look at the relative number of redder and bluer turnoff stars at $\alpha \sim 235$, $g^* = 17$ in Figure 8. Most of them are the redder population. Now look the model for $16.5 < r^* < 17.5$ in Figure 20. At $\alpha \sim 235$, somewhat more than half of the stars are MWTD, or the bluer population. We do note that qualitatively in the color-magnitude diagrams we see only two distinct turnoff colors, except in Figure 12 where there is a set of very bright stars with a very blue turnoff. We do not see a turnoff that gets steadily redder with increasing magnitude, or which widely varies as a function of position in the Galaxy (see, for example, stars with $0.2 < g^* - r^* < 0.5$ in Figure 8).

As with our model fits to Figure 19, the peak near the anticenter is not well centered on the model fits near $g^* = 18.5$. If we attempt to adjust our height above the plane to center the model, then the model becomes a very poor fit at the bright end. One could imagine that adding a warp to the MWTD might fix this discrepancy. Note in Figure 1 that there are multiple apparent overdensities of stars near the Galactic plane at the anticenter. At $\alpha \sim 125$, the overdensities are near $g^* = 15.5$ and $g^* = 19.5$. At $\alpha \sim 77$, the overdensities are near $g^* = 18$ and $g^* = 20$. We have no ready explanation for this.

Could all of this be explained without a disrupted dwarf galaxy or MWTD, but by warps or flares of the thick (or thin) disk? A warp in the disk means that the highest density of disk stars, which is generally in the Galactic plane ($b = 0^\circ$), shifts a little - to higher or lower Galactic latitude, depending on the direction. Such a warp has been detected in HI (Burton & te Lintel Hekkert 1986) and possibly in stars as well (Carney & Seitzer 1993; Alard 2001). The measured shifts amount to less than half a kiloparsec deviation from the $b = 0^\circ$ plane. Shifting the thick disk up or down by this amount could throw more or fewer stars into our dataset at any given location, but would not explain why the stars had a bluer turnoff than the supposed thick disk stars.

Disk flaring occurs if the scale height of the disk increases with cylindrical radius from the center of the Galaxy. This effect has also been seen in the Milky Way (Alard 2001) and perhaps in Andromeda (Guhathakurta, Choi, & Reitzel 2000). But again, increasing the scale height with Galactocentric radius also does not put stars all at the same distance from us, and also does not explain the bluer turnoff of these stars. We would expect to see the flare putting stars into our sample at even larger scale heights at slightly higher Galactic latitudes. We do not see an excess of stars at $g^* > 20$ and $b > 20^\circ$ near the anti-center. The excess stops at $g^* \sim 19.5$.

What we would need is a thick (or thin) disk which goes out to 14 to 18 kpc from the center of the Galaxy, then warps sharply perpendicular to the plane, goes up to about 20° Galactic latitude, and then ends abruptly. This would put stars all at the same distance from us (since we would be looking straight through the ‘disk’). The stars in this ‘disk’ must also have a turnoff with the same color as the spheroid population of stars in order to match the observations of Figure 24. Alternatively, one could construct a flare model which flares up 18 kpc from the center of the Galaxy, and then decreases in scale height with distance.

5.8. S52–32–20.4

A look at Figure 19 in directions near the Galactic center shows that one could not fit the observed density of stars at $\alpha = 240^\circ$ and $\alpha = 320^\circ$ without assuming a very flattened spheroid ($q = 0.5$). The exponential model is also a very flattened structure. The only way to avoid a very flattened spheroid is to postulate a large structure around $\alpha = 300^\circ$ which accounts for the star counts in this direction. A look at the distribution of magnitudes in this direction (Figure 21) shows that the magnitude distribution does not match our expectations for a power law spheroid, and thus there is the possibility of yet more structure at $\alpha = 320^\circ$. We identify this possible structure as S52–32–20.4.

We see below and in Table 2 that the stars in S52–32–20.4, which were originally assumed to be part of the spheroid population as well, appear to have significantly bluer turnoff stars than those of S6+41–20.0. This is a further indication that at least some of the stars in this direction are members of another Milky Way structure, and would release us from the need for a very flattened spheroid population.

If there is a stream at S52–32–20.4 that is not part of a smooth spheroidal distribution, then it is possible that we could fit a rounder $q = 0.8$ model, also shown in Figure 19.

5.9. Properties of the halo structures

From positions of the turnoffs in color-magnitude diagrams in the vicinity of the identified structures, selection criteria were chosen which were intended to favor each of the structures mentioned above. The specific selections shown in Figure 22 are: S223+20–19.4 and S200–24–19.8, black, ($7.05(g^* - r^*) + 17.24 < g^* < 21$ and $g^* - r^* > 0.1$); S341+57–22.5 (Sagittarius), blue, ($21.5 < g^* < 23.5$ and $-0.1 < g^* - r^* < 0.7$); S167–54–21.5 (Sagittarius), red, ($20.5 < g^* < 22.5$ and $0.0 < g^* - r^* < 0.6$); and S297+63–20.0, green, ($20.0 < g^* < 21.5$ and $0.1 < g^* - r^* < 0.4$). The star counts per area as a function of

right ascension for each of these selections are shown. Each datapoint on the plot represents the number of stars with the selection criteria in a region of the sky 2.5 degrees wide in declination by 0.5 degrees wide in right ascension. The curves were normalized to match near the Galactic center; the scale factor is indicated in the figure legend.

We can use this plot to estimate the number of turnoff stars in S167–54–21.5 (Sagittarius), for example. The peak of the red curve in the plot is at 1000 stars. Subtracting off a background of 400 stars, that leaves 600 stars at the peak. But the curve has been multiplied by a scale of 2, so there were only really 300 stars at the peak. The width of the structure is about 50 degrees, or 100 bins. Multiplying $0.5 \times 100 \times 300$ for the area of a triangle gives 15,000 turnoff stars spread over a $2.5 \times 50 = 125$ square degree area of sky.

The data curves in Figure 22 also show a possible peak in the stellar density at $\alpha \sim 10^\circ$. This is faintly evident in Figure 1, but is not distinguished from an extension of S167–54–21.5 (Sagittarius).

In addition to counting stars in stellar streams, it is interesting to look for directional information on the angle at which the streams cross the celestial equator. We split the equatorial data into three roughly equal declination bins: $\delta < -0.4^\circ$, $-0.4^\circ < \delta < 0.4^\circ$, and $\delta > 0.4^\circ$. The star counts in these bins are plotted as a function of right ascension in Figure 23. The center of S167–54–21.5 (Sagittarius) moves from $\alpha = 33^\circ$ to $\alpha = 36^\circ$ when the average declination goes from $\delta = -0.8$ to $\delta = 0.8$. The slope of this shift, $\Delta\delta/\Delta\alpha = 1.6/3 = 0.53$ is in excellent agreement with that predicted for the orbit of a Sagittarius stream at this position by Ibata et al. (2001b), where $\Delta\delta/\Delta\alpha \sim 0.5$. The northern Sagittarius stream structure, S341+57–22.5, appears to move towards lower right ascensions as the declination increases, which is the expected sign, though the magnitude of the shift is smaller than predicted, suggesting some overlapping of streams may be present here. The direction of S297+63–20.0 cannot be distinguished from a track perpendicular to the equator. The structures S223+20–19.4 and S200–24–19.8 shift slightly towards lower right ascensions as the declination increases.

The color of the turnoffs of the various overdensities provide an illuminating check on their identities. Figure 24 shows a the number of stars near the turnoff as a function of color for stars in the various identified structures. The structures plotted are: S167–54–21.5 (Sagittarius), $30^\circ < \alpha < 45^\circ$, $21 < g^* < 21.75$; S297+63–20.0, $180^\circ < \alpha < 195^\circ$, $20 < g^* < 20.75$; S223+20+19.4, $120^\circ < \alpha < 130^\circ$, $19.5 < g^* < 20.25$; S167–54–21.5, $70^\circ < \alpha < 80^\circ$, $19.25 < g^* < 20.0$; S52–32–20.4, $320^\circ < \alpha < 330^\circ$, $20.0 < g^* < 20.75$; S183+22–19.4, $100^\circ < \alpha < 125^\circ$, $19.5 < g^* < 20.25$, and the stars of the Sagittarius dwarf itself from Figure 6 with $22.25 < g^* < 23.0$. The counts for all curves have been normalized to peak at 1400. We chose the magnitude limits for each structure to produce the bluest possible

turnoff. Table 2 lists the colors of the turnoffs of the structures in $g^* - r^*$.

The black line shows the stars which are most likely from the spheroidal population of stars in the Galactic halo. (According to our definition, a MWTD would qualify as a spheroid population.) It is interesting that the turnoff of the Sagittarius dwarf, whose photometry has been scaled to match that of S341+57–22.5 (Sagittarius), is bluer than that of the spheroid population. Likewise, the turnoff of S167–54–21.5 is blue - further evidence that this overdensity is a part of the tidal stream of the Sagittarius dwarf galaxy. None of the other identified structures have turnoffs as blue as these.

S223+20–19.4, S218+22–19.5 and S183+22–19.4 have the same color turnoffs as the spheroid distributions. However, S200–24–19.8, which one could imagine might belong to the same halo structure as S223+20–19.4 and S183+22–19.4, has a much bluer turnoff. We believe the reason for this can be found in Figure 25, which shows the number counts of stars near the thick disk turnoff ($16.0 < g^* < 16.75$). Note that the turnoff $g^* - r^*$ color of presumed thick disk stars in all directions are within a couple of tenths of 0.4, except in the direction of S200–24–19.8, which is much bluer than the rest. (There are very few thick disk stars in the field of the Sagittarius Dwarf itself, which accounts for the apparently poor statistics of this curve.) If one adjusted the colors of the S200–24–19.8 turnoff stars by the amount needed for the thick disk turnoff in this direction to match all other directions, then the turnoff of S200–24–19.8 would more closely match the spheroid and S223+20–19.4, S183+22–19.4. We are uncertain as to the reason for the discrepancy, but believe that there is either a calibration error in these data, or the reddening correction could have been over-applied. If it is an error in the reddening correction which produced too blue a color by 0.05 magnitudes, then the g^* and r^* magnitudes should be shifted fainter by 0.15 and 0.10 magnitudes, respectively.

It is interesting that S297+63–20.0 appears to be intermediate in color between Sagittarius and the spheroid, as does S52–32–20.4. The latter is also a candidate for a flattened spheroid population.

6. Discussion

What have we learned about the halo of the Milky Way from all of this? The most important lesson is that at distances of 20 kpc from the center of the Galaxy, the stellar density is not at all smoothly varying, as a power law density distribution would be. It includes dwarf galaxies, globular clusters, and streamers of tidally stripped stars. With sufficiently large sky coverage, and good color photometry, these streamers can be identified

by their density in space, and not just by kinematic techniques which have been previously used to identify moving groups in the solar neighborhood.

The prevalence and ambiguity of clumped stars in our data frustrate our attempts to fit any smoothly varying ‘spheroidal’ distribution. The only direction in the sky in which the stellar distribution looks at all like our expectations for a power law distribution is at right ascension $240^\circ < \alpha < 250^\circ$, where the stars are less than 10 kpc from the Galactic center. In all other directions, the stellar distribution appears to be dominated by large structures with scale lengths of 10 kpc or greater, or by stars that do not fit neatly into the standard Galactic components. Even the stars near $\alpha = 245$ may not be identified as part of a presumed smooth power law distribution in the halo.

All of our attempts to fit a power law to the spheroid population of stars, both in magnitude and right ascension, produced best fits for a very flattened ($q \sim 0.5$) spheroid. We do not rule out a $q = 0.8$ spheroid, however, since we cannot be sure which of our data, if any, represents the spheroid distribution. We would also like to be clear that even if the spheroid is flattened, that does not imply a flattened halo dark matter distribution. One expects that stars and their associated dark matter are falling into the Galaxy from all directions.

The work of Kinman, Suntzeff, & Kraft (1994) is a recent work which found evidence for a flattened distribution of blue horizontal branch stars amongst other more spherically distributed populations of objects in the halo. This effect is discussed in Chiba & Beers (2001), and references therein, and suggests that a flattened halo dominates at $R < 15$ kpc, while the outer halo is spherical. We imagine that if one averaged over all of the streams, the distribution could be spherical at large Galactocentric radii. Close to the plane the MWTD or a flattened spheroid could dominate, and the distribution would appear to be flattened.

The overdensities which we have so far identified, and the smooth distributions of stars which we have assigned to some of the overdensities, do not account for all of the stars in the dataset. For example, look at the star counts in Figure 22 at $\alpha \sim 160^\circ$. There are significantly more stars here than in any model smooth model fit in Figure 19. We could try to construct a stream profile for S297+63–20.0 that put stars out this far. The spreading of tidal streams in the disruption process is not unexpected, especially if the mass distribution of the halo is not spherical. However, in this case the profile would seem contrived to fill in gaps between the assumed spheroid distribution at $\alpha \sim 250^\circ$ and the structure at $\alpha \sim 75^\circ$.

There are enormous streams of stars in the halo. The tidal stream from the Sagittarius dwarf galaxy is one of them. We may have found additional large streams as described in this paper. One might expect that there are streams from smaller infalling stellar associations, or

more dispersed streams from dwarf galaxies which were consumed by our Galaxy at earlier times in its history. These smaller or more dispersed streams might more naturally explain the difference in star counts between the models and the data at, for instance, $\alpha \sim 160^\circ$.

6.1. Debris from the Sagittarius dwarf

We have shown evidence supporting the identification of S341+57–22.5 and S167–54–21.5 with the tidal stream of the Sagittarius dwarf galaxy. The color-magnitude diagrams for the stars in these structures match that of the dwarf itself. Also, the $g^* - r^*$ color of the turnoff is consistent with that of the Sagittarius dwarf. We find no reason to doubt the identification of the structures at $\alpha \sim 210^\circ$ and $\alpha \sim 35^\circ$ as pieces of the stream of the Sagittarius dwarf galaxy.

One might ask whether any of the other structures identified in this paper could be part of the Sagittarius stream as well.

We assume from its low stellar density that the structure S297+63–20.0 has undergone tidal disruption in the Milky Way. It is possible that it could be a part of the tidal stream of the Sagittarius dwarf galaxy. Figure 2 of Ibata et al. (2001a) shows how debris from the Sagittarius dwarf is found off the main Sagittarius streamer orbit. If the F-stars in S297+63–20.0 are related to this off-stream debris, it implies a more dispersed stream than their $q = 0.9$ model predicts. A model closer to $q = 0.7$ is needed to explain the star density relative to that of S341+57–22.5 (Sagittarius) in terms of a single tidally precessed stream. Note, however, that the turnoff color of the stars in S297+63–20.0 do not support the idea that they originated in the Sagittarius dwarf galaxy. The turnoff color also does not rule out an identification with the Sagittarius stream; if they are associated it would imply that the stellar populations changed along a stream. It is also noteworthy that the S297+63–20.0 structure lies exactly on the plane of the Fornax-Leo-Sculptor dwarf galaxies (Majewski 1994), though it is much closer to the Galactic center than any of these dwarfs.

6.2. The Monoceros – Canis Major structure

The most tantalizing structures we have identified are S223+20–19.4, S218+22–19.5 and S183+22–19.4, which may be two sides of the same contiguous structure. S200–24–19.8 could also belong to this structure, but its relationship is more difficult to establish, due to the lower data quality in this region. Though it is possible that we have found three independent, similar structures of stars in the halo, we find that possibility unlikely. In §5.7 we explored

the possibility that this structure was part of a metal-weak thick disk. In this section, we explore the possibility that it is a tidally disrupted dwarf galaxy spread across 45° on the sky and 11 kpc from us (18 kpc from the center of the Galaxy). We believe this would not have been identified previously because it is so large and close, and it is hidden by the plane of the Milky Way. Figure 26 shows our knowledge of the edge of this stellar structure.

Since we do not probe the full extent of any structure in this area of the sky due to the intervening Galactic plane, it is difficult to distinguish a disrupted galaxy residual stream from a dwarf galaxy. Without kinematic information it is difficult for us to identify streams with possible parent dwarf galaxies. Since we do not see much of the perimeter of this structure, we cannot distinguish very easily between a dwarf galaxy and a gravitationally unbound streamer which circles the entire Galaxy at an inclination $i < 20^\circ$ to the Galactic plane (or something in between). Most other orbital directions are ruled out because it is only evident at the ends of stripes 10, 11, 12, 37, and 82.

A dwarf galaxy or disrupted galaxy stream of stars in the Galactic halo provides a simpler model which produces stars all at about the same distance from us. With a distance modulus of about 15.2 (from Figure 13 and an assumed absolute magnitude of $g^* = 4.2$), the distance to S223+20–19.4 is 11 kpc from the Sun. The same distance is derived for S183+22–19.4. These two overdensities are separated by 40° on the sky. If they indeed belong to the same structure, the structure is at least 8 kpc across. This is of the same scale as other large structures identified in the halo, including the Sagittarius dwarf spheroidal galaxy and the Sagittarius dwarf streamer. If S200–24–19.8 is part of the same structure, it is 8 kpc in the declination direction.

The width of the main sequence of S223+20–19.4 (see Figure 13) is only about one magnitude wide at $g^* = 21.1$. From the errors in color alone (multiply the expected dispersion in $g^* - r^*$ color $g^* = 21.1$, from Figure 3, by the slope of the main sequence in Figure 8), we could explain this entire width. To gain an upper limit on the thickness of the structure, we assume the entire one magnitude dispersion is due to depth of the structure, and obtain an upper limit for the depth of the structure of 6 kpc. We obtain a similar measurement for the depth of S183+22–19.4.

We now ask what the mass of a satellite in the Galactic plane would have to be in order to remain tidally bound. A simple tidal analysis can be done following, for example, equation 7.84 in Binney & Tremaine (1987). The mass of the satellite within the tidal radius is given by:

$$m_{sat} = 3M_{MW}\left(\frac{r_{tidal}}{D}\right)^3,$$

where r_{tidal} is the tidal radius of the dwarf, D is the distance of the satellite from the center of the Milky Way, and M_{MW} is the mass of the Milky Way within a radius of D . This

equation holds for $m_{sat} \ll M_{MW}$ and $r_{tidal} \ll D$. Plugging in $r_{tidal} = 4$ kpc and $D = 18$ kpc, we find that the satellite would have to have a mass equal to 3% of the mass of the Milky Way. Estimating the mass of the Milky Way interior to D from $M_{MW} = v_{MW}^2 D / G$ with $v_{MW} = 220$ km/sec, we find $M_{MW} = 2 \times 10^{11} M_{\odot}$, and an inferred satellite mass of $6 \times 10^9 M_{\odot}$.

For reference, the dynamically estimated initial mass of the Sagittarius dwarf galaxy is between 10^9 and $10^{11} M_{\odot}$ (Ibata and Lewis 1998; Jiang and Binney 2000), and it is currently about $10^9 M_{\odot}$ (Johnston et al. 1999a). Sagittarius is located 16 kpc from the Galactic center, and prolate with axis ratios 3:1:1 and a major axis of at least 9 kpc (Ibata et al. 1997). So far, our observations could be explained by a dwarf galaxy, similar in size to the Sagittarius galaxy, and hiding in the plane of the Milky Way 18 kpc from the Galactic center.

We now ask whether the star counts support the existence of so massive a structure in the halo. For stars of this turnoff color, $g^* - r^* = 0.28$, a relatively metal-poor, spheroidal type population with $[Fe/H] = -1.7 \pm 0.3$ is implied. An isochrone analysis like that for the Sagittarius stream of §4 then indicates that these turnoff stars typically would have masses near $0.75 M_{\odot}$ and approximate ages of 13 Gyr.

It is difficult to estimate the total number of stars in the proposed structure. If it is a dwarf galaxy, we have only detected the tails of the distribution. Star counts must be estimated by extrapolation. The highest detected stellar density is about 1500 F and G stars above background in a 1.25 square degree region of the sky (Figure 22). A structure with constant stellar density over a $40^{\circ} \times 40^{\circ}$ area of the sky would contain 2×10^6 stars. This is a lower limit.

If, instead, one fits to a model power law distribution ($\alpha = -3.5$) of stars centered half way between our two detections, such as that shown in Figure 13c and Figure 22, we calculate 1×10^7 F and G stars in the whole structure. If we put the center of the dwarf galaxy in the plane of the Milky Way, the inferred star count is several times higher. One could increase or decrease the inferred mass in stars by suitably adjusting the axial ratios or density profiles of the models. A mass in stars of a few times 10^8 solar masses is feasible, though by no means proven.

The total number of stars in the structure could easily be larger than these estimates if it is part of a stream which circles the Galaxy. If the stream contains at least 2×10^6 stars in the 40° section of sky where we detected it, and if it extends all the way around the Galaxy with similar density, it must contain at least 2×10^7 stars. The actual stellar and dynamical masses are likely to be much higher, since these estimates use the lowest possible extent and stellar densities.

Thus, the overdensity could indicate a dwarf galaxy in the constellation Monoceros or in nearby Canis Major to the South. However, even if it is a dwarf galaxy, the high tidal mass calculated above suggests that it would be in the process of disrupting, just as the Sagittarius dwarf galaxy is. One could go a step further, and suggest that what we have detected is not a dwarf galaxy at all, but is instead a gravitationally unbound stream of stars. This conclusion might be preferred, since it frees us from explaining the coincidence of having found the very ends of the structure by chance in stripes 10, 82 and 37. Figure 22 shows that even as a stream, this structure is significantly denser than the Sagittarius stream where it crosses zero declination. It is not only denser where we detect it, but it is also steeply rising as we run out of data.

If it is the result of the complete disruption of a gravitationally bound group of stars, the original mass of the infalling matter was probably quite large. The stream must contain at least 1×10^6 stars in the 40° section of sky where we detected it. If it extends all the way around the Galaxy with similar density, it must contain at least 1×10^7 stars. The actual stellar and dynamical masses are likely to be much higher, since these estimates use the lowest possible extent and stellar densities.

7. Conclusions

From stars in the Sloan Digital Sky Survey, we have shown that we can detect large (~ 10 kpc) structures of stars in the halo of the Milky Way. In Paper I, we showed that substructure in the Galactic halo could be identified from photometric data for blue stars. In this paper we extended the technique to identify large structures directly from turnoff stars. The color-magnitude diagrams of the stars in the structures should resemble the color-magnitude diagrams of the original dwarf galaxies or clusters which fell into the Milky Way. Features of the diagrams can be used to constrain the origins of each detected overdensity.

As more data are collected from the Sloan Digital Sky Survey, we will be able to trace each structure through space, and connect the overdensities in each stripe to each other to build up a large scale map of large stellar streams in the halo of our Galaxy. For now, we must be content to identify and name each overdensity, and only to estimate their full extent and origin. In this paper, we studied the $g^* - r^*$ colors and g^* magnitude distributions of seven overdensities of halo stars in the equatorial plane. We also show overdensities in three off-equatorial stripes, since they appear to be associated with the equatorial structures.

We emphasize these conclusions:

1. We show additional evidence that the overdensities S341+57–22.5 and S167–54–21.5

are in fact part of the tidal stream of the Sagittarius dwarf galaxy. These structures were discovered Paper I, and were interpreted by Ibata et al. (2001a) as two slices through the tidal stream of the Sagittarius dwarf galaxy.

The color-magnitude diagram of S341+57–22.5 bears striking resemblance to the color-magnitude diagram of the Sagittarius dwarf, including similar clumps of red stars. The color-magnitude diagram of S167–54–21.5 is consistent with that of the Sagittarius dwarf galaxy. In addition, the two overdensities are shown to have the same color turnoff stars as the Sagittarius dwarf galaxy; the turnoff of the Sagittarius dwarf is 0.08 to 0.1 magnitudes bluer in $g^* - r^*$ than the assumed Galactic spheroid stars, and substantially bluer than any other structure we have identified.

A comparison of the number of stars detected in the clump of red stars of S341+57–22.5 and S344+58–22.5 (in the adjacent stripe 11) with the number of similar stars in the Sagittarius dwarf indicate that we see about 1.5% of the present stellar mass of the Sagittarius dwarf in this 110 square degree area of the sky. This result assumes a constant clump star to stellar mass ratio between the Sagittarius dwarf and the stream.

2. From the spatial and magnitude distribution of turnoff stars in the spheroid, there is clear evidence for a diffuse structure S297+63–20.0, at a distance of about 20 kpc, extending over tens of degrees. Other evidence for this structure is a possible group of clustered RR Lyraes noted at the same distance and position by Vivas et al. (2001). This structure is very close in position to the Sagittarius dwarf tidal stream at S341+57–22.5, but two magnitudes brighter.

Although its proximity to the Sagittarius stream suggests that it might be another part of this same disrupted galaxy, the color of its turnoff ($g^* - r^* = 0.26$) is not the same. It is intermediate between that of the Sgr dwarf ($g^* - r^* = 0.22$) and that of the spheroid ($g^* - r^* = 0.28$). Surprisingly, the turnoff of S297+63–20.0 is nearly the same color as the turnoff of S52–32–20.4.

3. We observe many more stars at low Galactic latitudes near the Galactic anticenter than standard models predict at $g^* \sim 19.5$. These stars were selected to be bluer than the turnoff of the thick disk stars. Several of our identified structures lie in this general direction, and may be part of the same physical structure in the Galaxy. The structures S223+20–19.4, S218+22–19.5, S183+22–19.4, and with less significance S200–24–19.8, have similar color-magnitude diagrams, turnoff colors, and inferred distances. The similarity between the color-magnitude diagrams for S223+20–19.4 and S183+22–19.4 is particularly striking. The narrow main sequence seen in the color-magnitude diagrams is consistent with stars all at the same distance, about 11 kpc from the Sun. S223+20–19.4 and S183+22–19.4

are separated by 40° in right ascension. These are both separated from S200–24–19.8 by 40° in declination. The inferred spatial extent of the structure is 8 kpc in declination, centered approximately on the Galactic plane, by at least 8 kpc in right ascension. Since it would seem coincidental to have detected the structure exactly at its ends, we expect the structure is substantially longer than 8 kpc. The inferred distance from magnitudes of turnoff stars is 11-16 kpc from the Sun. From the magnitude distribution, the structure is less than 6 kpc thick along the line of sight. The turnoff stars of this structure have colors of spheroid stars ($g^* - r^* = 0.28$), rather than colors of thick disk stars ($g^* - r^* = 0.40$).

We propose two possible explanations for the unexpectedly high concentrations of blue stars near the Galactic anticenter. One of the possibilities is that they are stars associated with a tidally disrupted dwarf galaxy. The other is that these stars are part of an ‘even thicker disk’ population which has a bluer turnoff than the thick disk, a scale height of about 2 kpc, and a scale length around 10 kpc. Though neither explanation explains all of the data, either model could be reasonably extended to work. We do not propose that these possibilities exclude all other models - they are merely the most reasonable explanations we could find.

The tidally disrupted dwarf galaxy model neatly explains a distribution of stars all at the same apparent distance. The presence of the disrupted Sagittarius dwarf galaxy proves that such structures can and do exist in the Milky Way halo, and that they can be detected by these techniques. The inferred physical parameters for such a structure, though large, are not prohibitive; the projected mass of the original dwarf galaxy could be of similar size to the Sagittarius dwarf galaxy. This model does not explain why the stars we see toward the Galactic center show an unexpectedly large flattening (other additional streams or Galactic components are required to explain this), or why the turnoff of this proposed dwarf has the same color as the stars towards the Galactic center.

The ‘even thicker’ double exponential disk model uses large scale lengths to put the peak of the stellar density at faint enough magnitudes. This model is appealing because it naturally explains why such a structure is found over at least 40° of right ascension in the Galactic plane, and may correspond to the ‘metal-weak thick disk’ proposed by previous authors. The negatives of this model are that it does not fit the faint star counts near the Galactic center (Figure 18), and consumes all of the stars brighter than 20th magnitude which we expected were part of the power law spheroid part of the halo. This model would reduce the significance of, or eliminate, a power law distribution of halo stars. The distribution in magnitude of the concentration of stars near the anticenter is somewhat narrower than expected for an exponential disk (Figure 13).

Neither of these models explains the excess of stars at 15^{th} and 17^{th} magnitude near

the plane at the Galactic anticenter. A stream model might introduce additional streams to explain this, whereas a disk model might introduce warping to explain this.

4. On the other side of the Milky Way at $(l, b) = (52^\circ, -32^\circ)$, in a direction not far from the Galactic Center S52–32–20.4, there is evidence for stars distinct from a smooth spheroidal distribution of stars at $g^* = 20.8$. The distribution in magnitude is not consistent with a power law spheroid, although it could be fit with an exponential disk with large scale length. This is in contrast to the structure S6+41–20.0, which is the only observed concentration of halo stars that shows the spatial distribution, both in right ascension and apparent magnitude, expected for a power law Galactic spheroid. Additionally, the turnoff color of the stars in S52–32–20.4 is not the same as the presumed spheroid stars at S6+41–20.0, but rather intermediate between the spheroid and the Sagittarius dwarf.

If we try to fit a power law to both the stars in S6+41–20.0 and S52–32–20.4, then we must have $q < 0.6$ (and there is a poor fit with distance in the direction of S52–32–20.4). If this structure is regarded as distinct from the spheroid, then the remaining spheroidal stars towards the Galactic center could be fit with a rounder model, $q = 0.8$.

We do not present a single, coherent proposal for the components of the Milky Way, since it is not clear to what component each identified overdensity should be assigned. As more SDSS data is analyzed, and the extent of each structure is better known, we hope to generate a more coherent, defensible model.

5. Aside from the obvious large overdensities in the halo, there is tantalizing evidence for further, smaller structures, for example at $\alpha = 10^\circ$. One could imagine that there are even smaller structures which are not spatially resolved, which make up the difference between the observed star counts and the model fits to the spheroid population.

In this paper and in Paper I we identified seven or eight large overdensities which we believe might be associated with three or more halo structures. In view of these results, one must take seriously the possibility that there are many such previously unidentified structures in the halo. It is also probable that there are many smaller or more disrupted structures which might be better detected from kinematics than spatial information. Models of structure formation which have produced “too many galaxies per halo” may actually be predicting correct numbers of smaller halo structures. It appears we may be able to solve the problem by observationally finding more disrupted satellites in each halo.

One cannot help but wonder many things about the results presented in this paper. We conclude our discoveries with a list of questions for which we do not yet have answers. Is there a previously undiscovered dwarf galaxy hidden in the plane of the Milky Way? If there is a massive streamer or dwarf galaxy which orbits our Milky Way in the Galactic plane,

could this disrupt the disk at about 18 kpc from the Galactic center? Would it cause disk warping or flaring? Are there any dynamical models that could put a sheet of stars in a ring around the Galaxy without an infalling dwarf? If there is a structure with a scale length of many kiloparsecs which is only 11 kpc from us, can we detect any stars from this structure in the solar neighborhood kinematically or photometrically? Is there a metal-weak thick disk? Is there a model for the metal-weak thick disk which could explain why the stars seem to be shifted towards lower Galactic latitudes at $g^* \sim 18$? Why do we not see a break, or at least a gradient, in the turnoff color between stars which would nominally be assigned to the thin disk and those which would be assigned to the thick disk? Finally, are there any halo stars which form a well-mixed, smooth, spheroidal distribution, and were any of them formed during the initial collapse of our Galaxy, as was proposed by Eggen, Lynden-Bell, and Sandage (1962)?

We acknowledge useful comments from Hugh Harris, Daniel Eisenstein, Amina Helmi, Doug Whittet and David Weinberg. We appreciate the close reading and extensive comments of the anonymous referee, which substantially improved the paper.

The Sloan Digital Sky Survey (SDSS) is a joint project of The University of Chicago, Fermilab, the Institute for Advanced Study, the Japan Participation Group, The Johns Hopkins University, the Max-Planck-Institute for Astronomy (MPIA), the Max-Planck-Institute for Astrophysics (MPA), New Mexico State University, Princeton University, the United States Naval Observatory, and the University of Washington. Apache Point Observatory, site of the SDSS telescopes, is operated by the Astrophysical Research Consortium (ARC).

Funding for the project has been provided by the Alfred P. Sloan Foundation, the SDSS member institutions, the National Aeronautics and Space Administration, the National Science Foundation, the U.S. Department of Energy, the Japanese Monbukagakusho, and the Max Planck Society. The SDSS Web site is <http://www.sdss.org>.

REFERENCES

- Alard, C. 2001, preprint astro-ph/0007013
- Bahcall, J. N. & Soneira, R. M. 1984, *ApJS*, 55, 67
- Binney, J., Gerhard, O., & Spergel, D. 1997, *MNRAS*, 288, 365
- Binney, J., & Tremaine, S. 1987, “Galactic Dynamics”
- Bullock, J. S., Kravtsov, A. V., and Weinberg, D. H. 2001, *ApJ*, 548, 33
- Burton, W. B., & te Lintel Hekkert, P. 1986, *A&AS*, 65, 427
- Buser, R., Rong, J., Karaali, S. 1999, *A&A*, 348, 98
- Cardelli, J. A., Clayton, G. C., & Mathis, J. S. 1989, *ApJ*, 345, 245
- Carney, B. W. & Seitzer, P. 1993, *AJ*, 105, 2127
- Chen, B. et al. 2001, *ApJ*, 553, 184
- Chiba, M. & Beers, T. C. 2000, *AJ*, 119, 2843
- Chiba, M. & Beers, T. C. 2001, *ApJ*, 549, 325
- Cohen, M. 1995, *ApJ*, 444, 874
- Dohm-Palmer, R. C., Helmi, A., Morrison, H., Mateo, M., Olszewski, E. W., Harding, P., Freeman, K.C., Norris, J., & Shectman, S. A. 2001, *ApJ*, in press (astro-ph/0105536)
- Eggen, O. J., Lynden-Bell, D., and Sandage, A. R. 1962, *ApJ*, 136, 748
- Friel, E. D. 1995, *ARA&A*, 33, 381
- Frogel, J. A. 1999, *Ap&SS*, 265, 303
- Frogel, J. A. 1988, *ARA&A*, 26, 51
- Fukugita, M., Ichikawa, T., Gunn, J. E., Doi, M., Shimasaku, K., Schneider, D. P. 1996, *AJ*, 111, 1758
- Gilmore, G., Wyse, R. F. G., & Kuijken, K. 1989, *ARA&A*, 27, 555
- Gilmore, G., & Reid, N. 1983, *MNRAS*, 202, 1025
- Guhathakurta, P., Choi, P.I., & Reitzel, D. B. 2000, *BAAS*, 197, 3702

- Gunn, J. E. et al. 1998, *AJ*, 116, 3040
- Hammersley, P. L., Garzon, F., Mahoney, T., & Calbet, X. 1995, *MNRAS*, 273, 206
- Helmi, A., White, S. D. M., de Zeeuw, P. T., and Zhao, H. 1999, *Nature*, 402, 53
- Helmi, A., & White, S. D. M. 2001, *MNRAS*, 323, 529
- Hess, R. 1924 “The Distribution Function of Absolute Brightness”, in Seeliger Festschrift, ed. H. Kienle (Berlin, Springer), 265
- Humphreys, R. M. & Larsen, J. A. 1995, *AJ*, 110, 2183
- Ibata, R., Irwin, M., Lewis, G. F., Stolte, A. 2001a, *ApJ*, 547, L133
- Ibata, R., Lewis, G. F., Irwin, M., Totten, E., and Quinn, T. 2001b, *ApJ*, 551, 294
- Ibata, R. A. and Lewis, G. F. 1998, *ApJ*, 500, 575
- Ibata, R. A., Wyse, R. F. G., Gilmore, G., Irwin, M. J., Suntzeff, N. B. 1997, *AJ*, 113, 634
- Ibata, R. A., Gilmore, G., and Irwin, M. J. 1995, *MNRAS*, 277, 781
- Ibata, R. A., Gilmore, G., and Irwin, M. J. 1994, *Nature*, 370, 194
- Ivezić, Z., et al. 2000, *AJ*, 120, 963
- Jiang, I. and Binney, J. 2000, *MNRAS*, 314, 468
- Johnston, K. V., Majewski, S. R., Siegel, M. H., Reid, I. N., Kunkel, W. E. 1999a, *AJ*, 118, 1719
- Johnson, K. V., Zhao, H., Spergel, D. N., and Hernquist, L. 1999b, *ApJ*, 512, L109
- Johnston, K. V., Sigurdsson, S., Hernquist, L. 1999, *MNRAS*, 302, 771
- Johnston, K. V., Hernquist, L., and Bolte, M. 1996, *ApJ*, 465, 278
- Johnston, K. V., Spergel, D. N., Hernquist, L. 1995, *ApJ*, 451, 598
- Kinman, T. D., Suntzeff, N. B., & Kraft, R. P. 1994, *AJ*, 108, 1722
- Klypin, A. A., Kravtsov, A. V., Valenzuela, O., & Prada, F. 1999, *ApJ*, 522, 82
- Kerber, L. O., Javiel, S. C., & Santiago, B. X. 2001, *A&A*, 365, 424
- Larsen, J. A., & Humphreys, R. M. 1996, *AJ*, 468, 99

- Layden, A., & Sarajedini, A. 2000, AJ, 119, 1760
- Lupton, R. H., Gunn, J. E., & Szalay, A. S. 1999, AJ, 118, 1406
- Lupton, R. H., et al., AJ, in preparation
- Lynden-Bell, D., and Lynden-Bell, R. M. 1995, MNRAS, 275, 429
- Majewski, S. R., Siegel, M. H., Kunkel, W. E., Reid, I. N., Johnston K. V., Thompson, I. B., Landolt, A. U., and Palma, C. 1999, AJ, 118, 1709
- Majewski, S. R., Munn, J. A., and Hawley, S. L. 1996, ApJ, 459, L73
- Majewski 1994, ApJ, 431, 1
- Majewski, S. R. 1993, ARA&A, 31, 575
- Marconi, G., Buonanno, R., Castellani, M., Iannicola, G., Molaro, P., Pasquini, L., and Pulone, L. 1998, A & A, 330, 453
- Martinez-Delgado, D., Aparicio, A., Gomez-Flechoso, M. Angeles, & Carrera, Ricardo 2001, ApJ, 549, L199
- Mendez, R. A. & van Altena, W. F. 1998, A&A, 330, 910
- Morrison, H. L., Flynn, C., & Freeman, K. C. 1990 AJ, 100, 1191
- Moore, B., Ghigna, S., Governato, F., Lake, G., Quinn, T., Stadel, J., & Tozzi, P. 1999, ApJ, 524, L19
- Norris, J. E. 1999, Ap&SS, 265, 213
- Norris, J. E. 1994, ApJ, 431, 645
- Odenkirchen, M. et al. 2001, ApJ, 548, L165
- Ojha, D. K., Bienayme, O., Robin, A. C., Creze, M., Mohan, V. 1996, 311, 456
- Pier, J., Munn, J. A., Kent, S. M., et al. 2001, AJ, in preparation
- Reid, N. & Majewski, S. R. 1993, ApJ, 409, 635
- Reyle, C., & Robin, A. C. 2001, A&A, 373, 886
- Robin, A. C., Haywood, M., Creze, M., Ojha, D. K. & Bienayme, O. 1996, A&A, 305, 125

- Schlegel, D.J., Finkbeiner, D.P., & Davis, M. 1998, ApJ, 500, 525
- Scranton, R., Johnston, D., & Lupton, R. H. 2001, AJ, submitted.
- Smith et al., in preparation
- Stoughton, C., et al. 2001, AJ, in press
- Vivas, A. K. et al. 2001, ApJ, 554, L33
- Wyse, R. F. G. 1999, Baltic Astronomy, 8, 593
- Yanny, B., Newberg, H. J., et al. 2000, ApJ, 540, 825 (Paper I)
- York, D.G. et al. 2000, AJ, 120, 1579

Fig. 1.— Two dimensional (g^* and RA) polar coordinate-density histogram of turn-off stars on the celestial equator with $0.1 < g^* - r^* < 0.3$. The shading of each cell indicates the relative number counts of stars in each (RA, g^*) bin. Typical absolute magnitudes of stars with these colors are $M_{g^*} = +4.2$, and thus stars with $g^* = 19.4$ are at distances of 11 kpc from the Sun. $g^* = 22.5$ corresponds to objects 45 kpc from the Sun. The center of the Galaxy ($l = 0$) is towards the lower left at $\alpha = 228^\circ$. The intersection of the plane of the Celestial equator with the Galactic plane ($b = 0$) is indicated by the bold, black line. Note the numerous high signal-to-noise structures existing in the halo of the Milky Way. Boldface labels indicate positions of overdensities which are discussed in the text. The color cut excludes most thick disk stars. The feature at $\alpha = 60^\circ$ is probably an artifact of the reddening correction applied to the data, since there is a large dust cloud at this position. The streak at $\alpha = 229^\circ$ is due to Pal 5. The grey scale bar at the bottom of the figure indicates relative star count density in each pixel.

Fig. 2.— Reddening and quasar candidate counts vs. RA on the celestial equator ($-1.26 < \delta < 1.26$). $E(B-V)$ at $\delta = 0$ (scaled $\times 10$) is shown to indicate areas where dust may affect the object selection. The quasar candidates are all the stellar objects in the color box $18 < g^* < 21.5, 0 < u^* - g^* < 0.3, 0.1 < g^* - r^* < 0.3$. The fact that the quasar candidate counts are generally uniform around the equator indicates that selection of F stars as a function of α is also uniform.

Fig. 3.— Limiting magnitude and completeness for three color ranges, and also $g^* - r^*$ errors vs. color. Stars in overlapping runs were matched based on position (within $2''$). Then stars in the first run with colors in the three ranges indicated were examined for matches (of any color) in the other run as a function of magnitude. The plotted results (with binomial distribution error bars shown) indicate completeness independent of color to about $g^* \sim 22.5$. Shown as crosses are rms errors in $g^* - r^*$ for objects with $g^* - r^* < 1$ as determined from matching objects.

Fig. 4.— Color-Magnitude diagram of objects typed as galaxies in the SDSS sample. Normally, color-magnitude diagrams are shown with one dot plotted for each star observed. Since we have too many stars to be effectively plotted in this way, we instead histogram the number of counts in each 2-D binned cell. The horizontal bin width in $g^* - r^*$ color is 0.02 magnitudes, and the vertical bin width in g^* is 0.05 magnitudes. The image is plotted with square root density scaling. The galaxies are localized in color magnitude space redward of the turnoff in such a way that they do not contaminate blue star counts at $g^* < 22.5$.

Fig. 5.— Color-magnitude image of S341+57–22.5 (Sagittarius). This shows stars in the equatorial region $200^\circ < \alpha < 225^\circ$, with binning in color and magnitude identical to Figure 4.

Capturing the color-magnitude diagram as an image allowed us to subtract off images of other parts of the sky which do not contain the Sagittarius dwarf streamer, as detailed in the text. The image clearly shows a turnoff at about $g^* = 22.5$, a giant branch extending to a clump of red stars at $g^* = 19.7$, a blue horizontal branch extending from the clump to as blue as $g^* - r^* = -0.1$, and blue stragglers which extend from the turnoff up through the horizontal branch.

Fig. 6.— Color-magnitude image of Sagittarius dwarf. The stellar data used to create this color-magnitude image comes from Marconi et al. (1998), who published photometry for two fields in the Sagittarius dwarf itself, using V and I filters on the 3.5 m ESO-NTT telescope. In order to compare this data with Figure 5, the photometry was converted to the SDSS filter system and the magnitude shifted to reflect the difference in distance between the Sagittarius dwarf stream (at this position) and the Sagittarius dwarf galaxy. The similarity between the color-magnitude diagram of the Sagittarius dwarf and that of the streamer in Figure 5 is striking.

Fig. 7.— Color-magnitude image of S167–54–21.5 (Sagittarius). We used data from stripe 82, $15^\circ < \alpha < 50^\circ$ to make a color-magnitude image, and then subtracted suitable reference fields to decrease the contrast between the streamer stars and the other stars of the Galaxy. The southern streamer shows a clear turnoff, giant branch, and blue straggler stars. The horizontal branch at $g^* \sim 18$ is rather weak, and the clump of red stars is neither ruled out nor apparent. The color-magnitude diagram is consistent with its identification as a piece of the Sagittarius streamer, though we cannot make a positive identification from this diagram.

Fig. 8.— Color-magnitude image of stars in stripe 10 with $230^\circ < \alpha < 240^\circ$ (S6+41–20.0, spheroid).

Fig. 9.— Excess stars in S167–54–21.5 (Sagittarius) as a function of apparent g^* magnitude. This shows all of the stars in stripe 82 with $0.1 < g^* - r^* < 0.3$ and $30^\circ < \alpha < 45^\circ$, with all of the stars in $20^\circ < \alpha < 25^\circ$ and $45^\circ < \alpha < 55^\circ$ subtracted off. We use the apparent magnitude of the turnoff stars from this plot plus the distance modulus to S167–54–21.5, as determined from horizontal branch stars, to estimate that the turnoff stars have $M_{g^*} \sim +4.2$.

Fig. 10.— Models of power law and exponential disk profiles as they intersect the celestial equator. Four smooth models are shown. a), b) and c) are power law models with $\alpha = -3.5$ and flattening $q=(0.5, 1.0, 1.5)$, respectively. d) shows an exponential disk model with a scale length of 3 kpc and a scale height of 1 kpc. All models assume a narrow (delta-function) population of F main sequence stars of absolute magnitude $M_{g^*} = 4.0$ for power law models

and $M_{g^*} = 4.5$ for the exponential disk model. These absolute magnitudes were chosen to put stars at about the right apparent magnitude near the anticenter, and are not too far off from the absolute magnitude we expect for stars in Figure 1.

Fig. 11.— Hess diagram for stars in stripe 10 with $180^\circ < \alpha < 195^\circ$ (Spheroid).

Fig. 12.— Hess diagram for stars with $117^\circ < \alpha < 130^\circ$ S223+20–19.4. Note the turnoff near $g^* \sim 19.4$ which is distinct from the brighter thin/thick disk stars at $g^* < 18.5$. This structure appears to be the main sequence of a localized (in distance) distribution of stars about 11 kpc from the Sun in the direction of $(l,b) = (220^\circ, 20^\circ)$.

Fig. 13.— Model fits to the data at $122^\circ < \alpha < 130^\circ$ (S223+20–19.4). In a) six power law models are plotted. In b) six exponential disk models are plotted. Models and data are arbitrarily normalized. Note how broad in magnitude these distributions are compared to the peak of the distribution of observed stars in c). None of the models of a) or b) fit the data well, though an exponential disk model with scale height ~ 2 kpc and scale length ~ 10 kpc might be made to work by postulating brighter and fainter peaks in the star counts from other populations. In c) we also show a distribution of redder stars. The redder color cut includes thick disk stars at the bright end, and an even narrower peak (the peak is fainter because the selected stars are intrinsically fainter). A model spheroid offset from the center of the Galaxy by about 18 kpc in the direction of the excess stars is fit to the data. One expects the broader peak in the data than in the model due to intrinsic spread in the absolute magnitudes of the stars, plus photometric error.

Fig. 14.— Model fits to the data at $70^\circ < \alpha < 77^\circ$ (S200–24–19.8). Same as Figure 13, except on the other side of the Galactic plane. Again, the power law models look nothing like the data. Exponential disk models are better, but have a somewhat broader distribution and require larger scale lengths than typically assumed for the thick disk.

Fig. 15.— Hess diagram for stars on the end of stripe 82 with $70^\circ < \alpha < 77^\circ$ (S200–24–19.8).

Fig. 16.— These 2D histograms of F star density are made in the same way as those in Figure 1. Data from stripes 37 (upper), and 12 (lower) are shown. An excess of stars at $g^* \approx 19.4, b \sim +20^\circ$ is seen in each plot. These stars all have color-magnitude diagrams similar to that of Figure 12, and may be pieces of a vast structure (dwarf companion or large scale length exponential disk).

Fig. 17.— Hess diagram for stars on the end of stripe 37, with $\alpha < 125^\circ$ (S183+22–19.4). Note the similarity to the Fig 12. The horizontal branch at $g^* \sim 20.5, g^* - r^* \sim -0.2$ is from

the globular cluster NGC 2419.

Fig. 18.— Model fits to the data at $230^\circ < \alpha < 240^\circ$ (Spheroid). Here the flattened power law model $q = 0.5$ is a good fit to the data (the normalization of the models is arbitrary). Note in particular that no exponential disk model is a good fit. If we wish to explain the structure in Figure 13c with a smooth, exponential disk distribution of spheroid stars, one must modify the functional form of the spheroid or add a separate component in the general direction of the Galactic center.

Fig. 19.— F star counts along the celestial equator. We show number counts of stars in stripe 10 and 82 with $20.0 < g^* < 21.5$ and $0.1 < g^* - r^* < 0.4$ (black). The data are binned in half degree bins in right ascension. Since the stripe is 2.5 degrees wide, the number counts are per 1.25 square degrees. We also show models for exponential disk and power laws, scaled to best match the data. None of the power law models put large numbers of stars near the Galactic anticenter. It is possible to put stars near the plane and the anticenter with an exponential disk model. Also a prolate spheroid centered out at $(X, Y, Z) = (-17.4, -4.3, 1.1)$, which could represent a dwarf spheroidal galaxy, is shown in magenta. This is a very good fit to the data near $\alpha = 100^\circ$. We can then then fit the stars near $\alpha = 280^\circ$ with a power law model, but only if it is very oblate. If we wanted to represent the spheroid by a more spherical power law, then the stars near $\alpha = 320^\circ$ would need to be explained by a different Galactic component.

Fig. 20.— Thin disk plus extended metal weak thick disk model of the Galaxy. We show F/G turnoff star counts as a function of right ascension, on the Celestial Equator, for five magnitude ranges. The stars were color selected, with $0.2 < g^* - r^* < 0.5$. The data is indicated by black dots. The solid lines show theoretical exponential disks fit to the data. The standard (black) and proposed (red) thin+thick exponential disk models are normalized to match the star counts at $\alpha = 240^\circ$ in the $16.5 < g^* < 17.5$ plot. A ‘standard model’ for the thick and thin disk, with thin disk scale height 250 pc, thin disk scale length 2.5 kpc, thick disk scale height 1.0 kpc and thick disk scale length 3.0 kpc, is shown in black. The assumed ratio of thin disk stars to thick disk stars at the solar position is 1:30. This model does not account for the large number of faint stars near the Galactic anticenter. Adding a power law spheroid to this would only make the disagreement larger. In red we show a model with a thin disk with scale height 200 pc and scale length 2.8 kpc, plus a proposed metal weak thick disk with scale height 1.8 kpc and scale length 8 kpc. The ratio of thin disk to MWTD stars at the solar position is 100:1. The thin disk and MWTD components of this model are shown in green and blue, respectively. One could achieve a similar fit to the data if a third double exponential, representing a standard thick disk, is included in the model. It is difficult to fit the peaks near the center and anticenter by including both standard power

law and MWTD components. The power law inserts too many stars near the Galactic center (and very few towards the Galactic anticenter) at faint magnitudes.

Fig. 21.— Disk and Halo models vs. data at $320^\circ < \alpha < 330^\circ$ S52–32–20.4. Note that this distribution is not consistent with a power law spheroid. To fit this distribution with an exponential disk would require large scale lengths.

Fig. 22.— Selected F star counts along the celestial equator. We show the relative distribution of stellar densities along the celestial equator. Four boxes in color-magnitude space were chosen to highlight stars in each of the detected overdensities (S167–54–21.5 (Sagittarius) red; S223+20–19.4 black; S297+63–20.0 green; and S341+57–22.5 (Sagittarius) blue. Curves were scaled so that they match in height at $\alpha = 240^\circ$. Notice that each detected overdensity produces a strong peak in this plot. There is an additional overdensity apparent in this plot at $\alpha = 10^\circ$. One could imagine other smaller overdensities that could help fill in the plot between the theoretical curves and the data curves. The dip in star counts in the center of the structure at $\alpha = 213$ is artificially caused by a decrease in the data quality in this region. The very low points occur where the data quality was so low that the data in close to half a degree of one of the runs was removed.

Fig. 23.— Stream direction. The SDSS data are obtained in stripes of width 2.5 degrees in declination. To examine the direction that a stream of stars makes with a stripe, we divide each stripe up into three sub-stripes, each with width 0.8° in declination. The histogram of star counts within each sub-stripe is shown for a) S167–54–21.5 (Sagittarius), b) S341+57–22.5 (Sagittarius), c) S297+63–20.0 and d) S223+20–19.4. Each plot shows the stars which have colors and magnitudes consistent with the clumped population (see §5.9). For the S167–54–21.5 (Sagittarius) structure a shift is apparent from south to north and indicates that the stream crosses the celestial equator at an angle of $PA \sim 30^\circ$. A shift in the opposite direction (as would be expected for the stream) is observed in S341+57–22.5. The peak at $\alpha = 229^\circ$ is due to the globular cluster Pal 5. In this figure, the counts in a single three degree bin have been divided by 0.925 to compensate for missing data in right ascension range $215.5 < \alpha < 215.95$. This data was flagged as bad data and was removed from our dataset. Data near this right ascension has poorer than average seeing. The density of stars in S223+20–19.4 decreases for increasing declination. Since we do not detect the a peak for structure S223+20–19.4, we cannot tell whether this is a shift or a density change in the declination direction. If it is a shift, it is consistent with a structure which is aligned more along the Galactic plane than along the celestial equator.

Fig. 24.— Color cuts of stars in the vicinity of the turnoff for several populations (isolated in α and g^* magnitude) of stars. The peak of the histogram for each population gives the color

of the main sequence turnoff of each population. Populations with the same turnoff colors may be of the same age and metallicity and may be associated. S167–54–21.5 (Sagittarius), magenta; and S341+57–22.5 (Sagittarius – not shown) both have turnoffs well to the blue of $g^* - r^* = 0.25$, and are probably of the same origin. S297+63–20.0 stars (blue) and S52–32+20.4 stars (green) also have similar turnoff colors $g^* - r^* \sim 0.26$. The turnoff stars of the spheroid (black), S183+22–19.4 (red), S218+22–19.5 (red) and S223+20–19.4 (red) all have similar distributions, while that of the S200–24–19.8 structure (cyan) has a bluer turnoff. This bluer color of S200–24–19.8 might be the result of calibration errors or too much reddening correction applied here (see Figure 25).

Fig. 25.— Same as Fig 24, except stars with thick and thin disk magnitude cuts ($g^* \sim 17.5$) were selected. Note the peaks of the histograms are in concordance except for that of S200–24–19.8 (cyan) which is too blue in $g^* - r^*$. This suggests that too much reddening correction may have been applied to the data points in this region where estimated $E(B - V) \sim 0.12$.

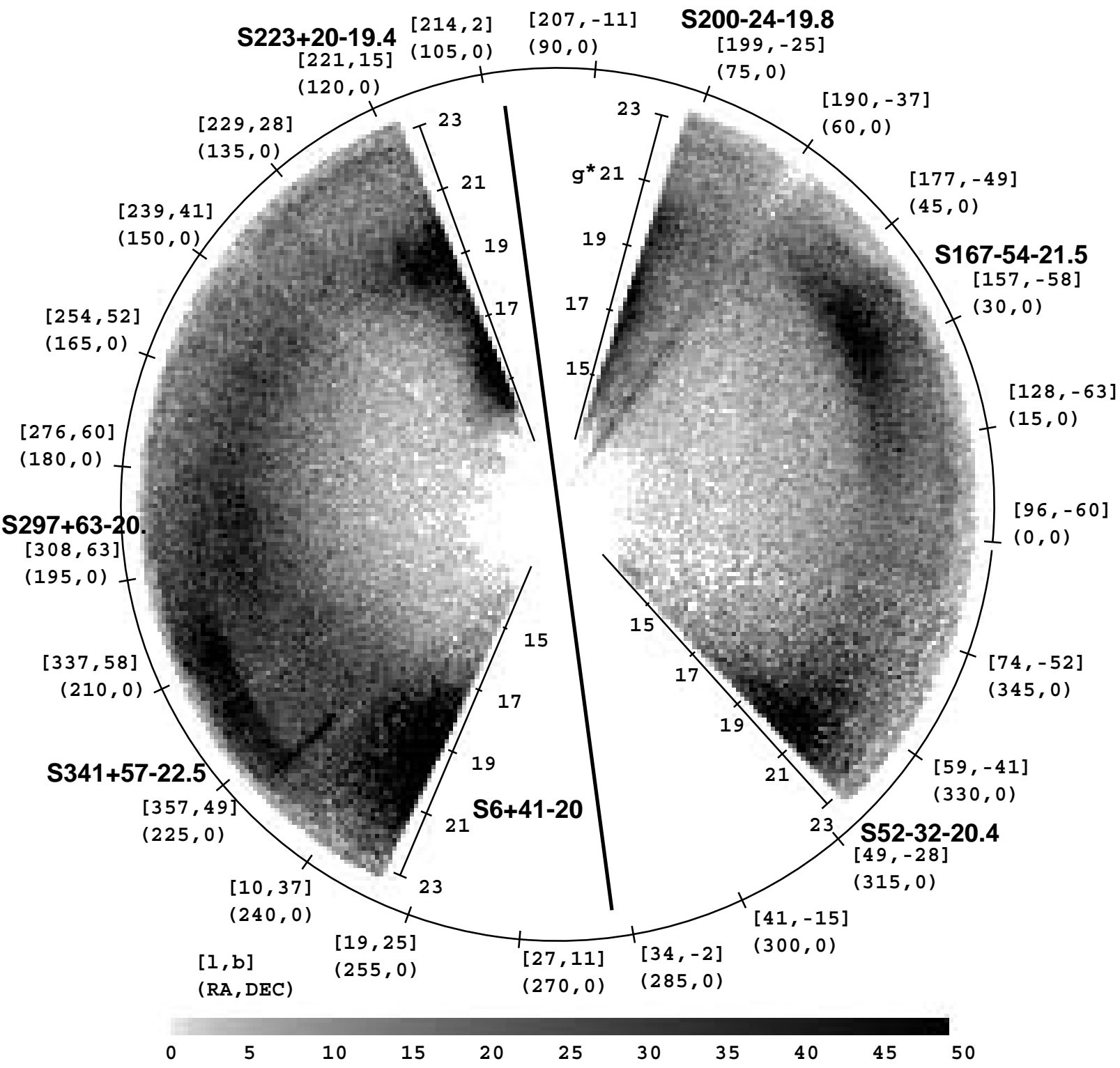
Fig. 26.— Sketch of the ends of stripes 37, 12, 10, and 82 in Galactic (l,b). Shading shows the distribution of stars in a color-magnitude selection chosen to favor objects in the S223+20–19.4 and S200–24–19.8) structures (see §5.9). Black shading denotes 600 stars per square degree or more with this selection. Grey shading denotes 400 stars per square degree or more. The excess of stars near the ends of these stripes are not associated with known thin disk, thick disk or halo populations and may be part of the same large structure near the Galactic anti-center at an implied distance of 18 kpc from the Galactic center.

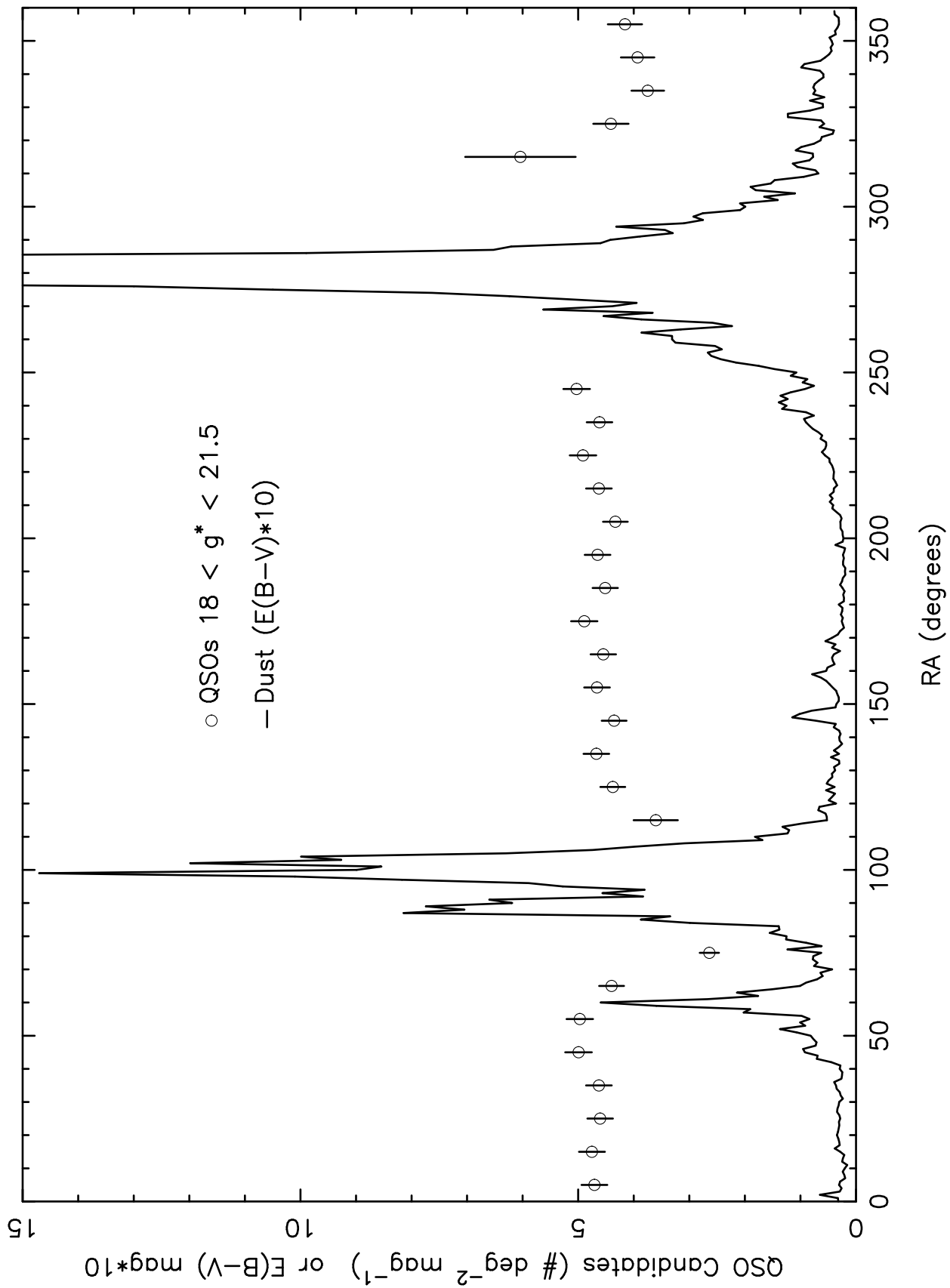
Table 1 - Observing Log Summary – Equatorial data

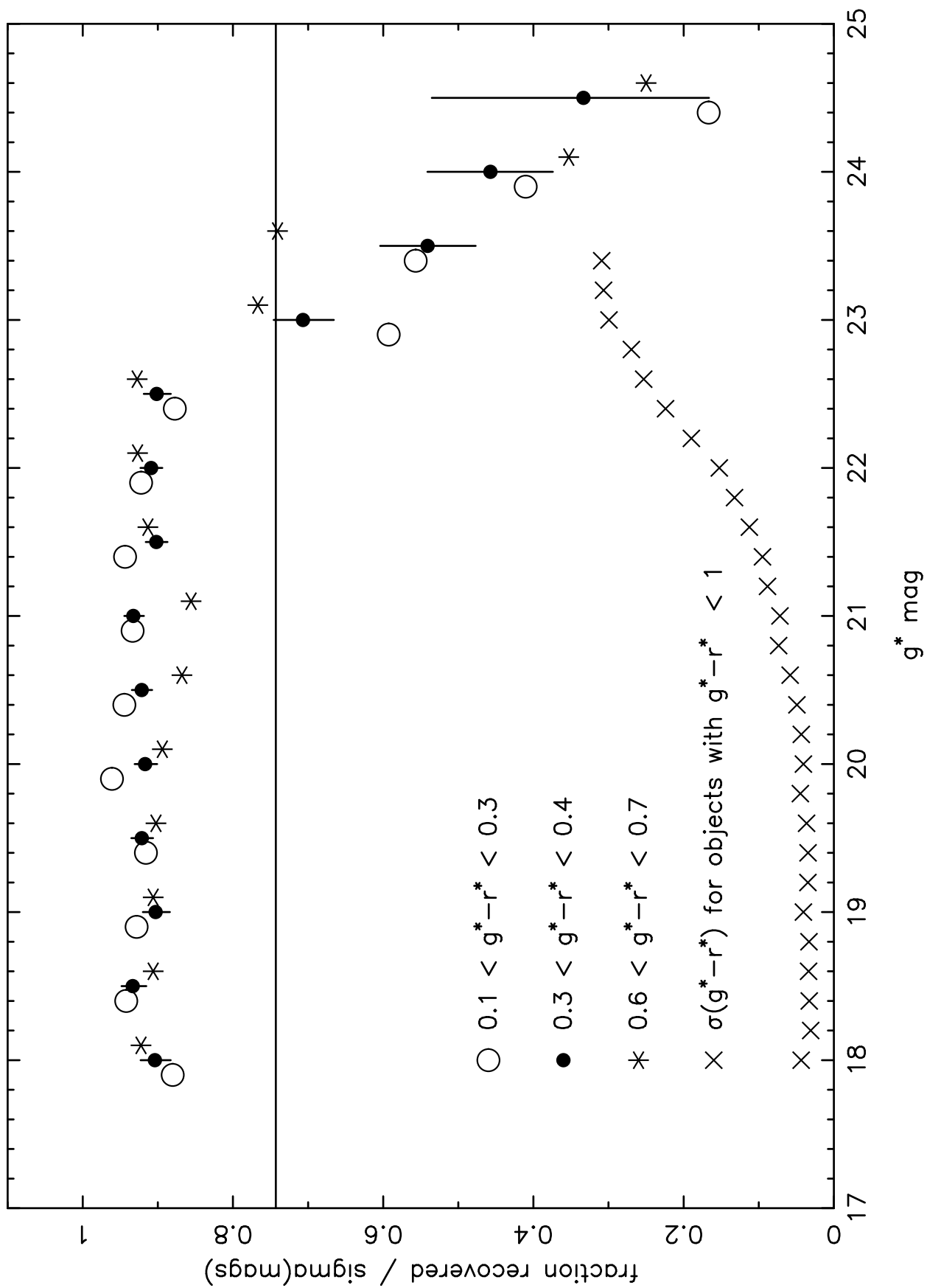
Run	Stripe	Strip	Date	Start RA (deg)	End RA (deg)	Seeing (arcsec)	Mult
94	82	N	1998 Sep 19	350	56	1.7	1
125	82	S	1998 Sep 25	350	77	1.9	1
752	10	S	1999 Mar 21	145	233	1.4	1
752	10	S	1999 Mar 21	234	250	1.4	2
756	10	N	1999 Mar 22	117	121	1.4	2
756	10	N	1999 Mar 22	122	235	1.4	1
1350	37	S	2000 Apr 6	112	125	1.5	1
1402	37	S	2000 Apr 27	112	125	1.5	1
1450	37	S	2000 May 3	112	125	1.5	1
1462	11	S	2000 May 5	120	137	1.5	1
1752	82	N	2000 Oct 1	56	77	1.5	1
1755	82	S	2000 Oct 2	319	350	1.4	2
1907	11	N	2000 Nov 30	120	137	1.4	1
2125	12	S	2001 Feb 20	122	135	1.5	1
2126	12	N	2001 Feb 20	122	135	1.5	1

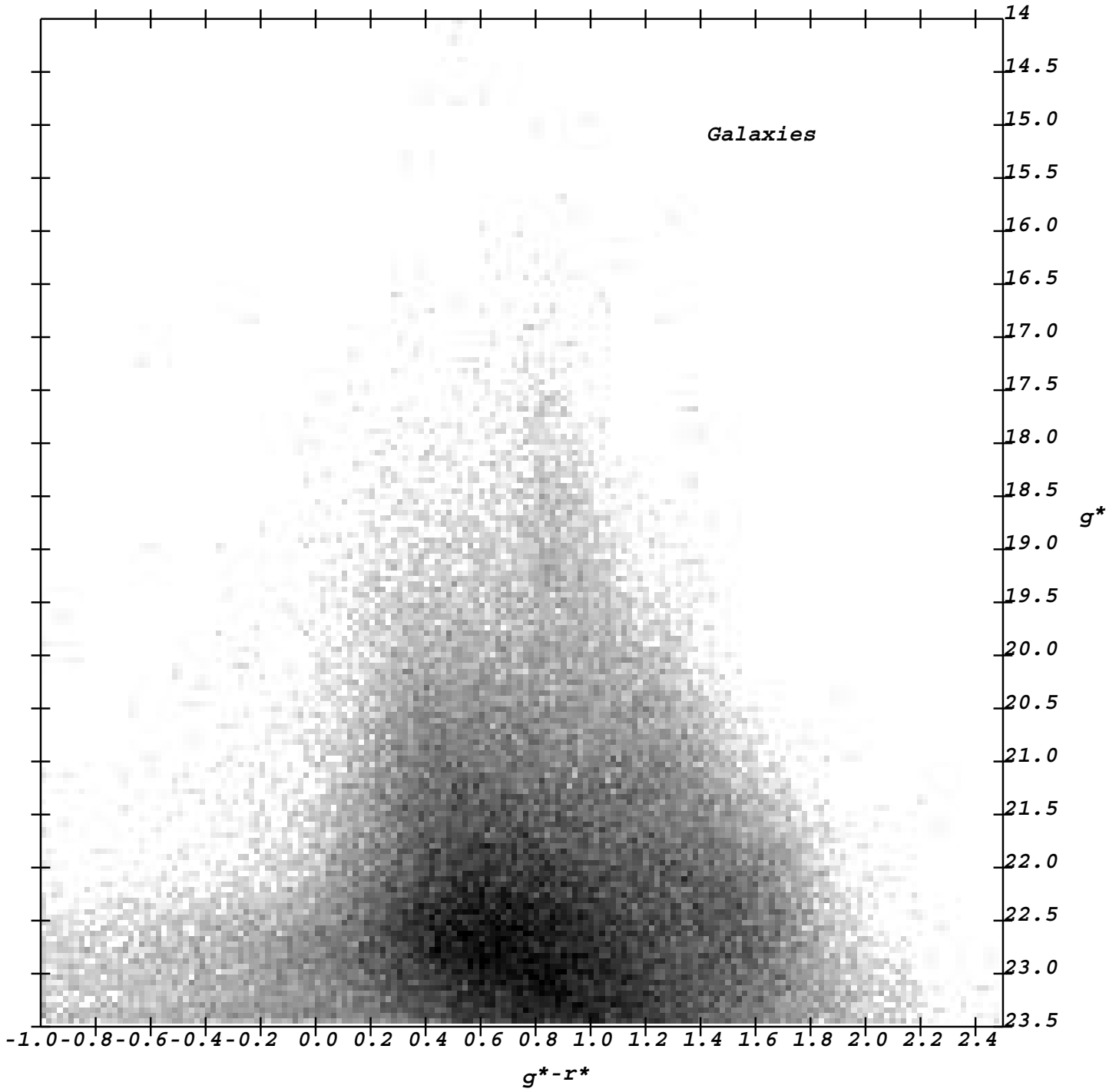
Table 2 - Summary of observed structures

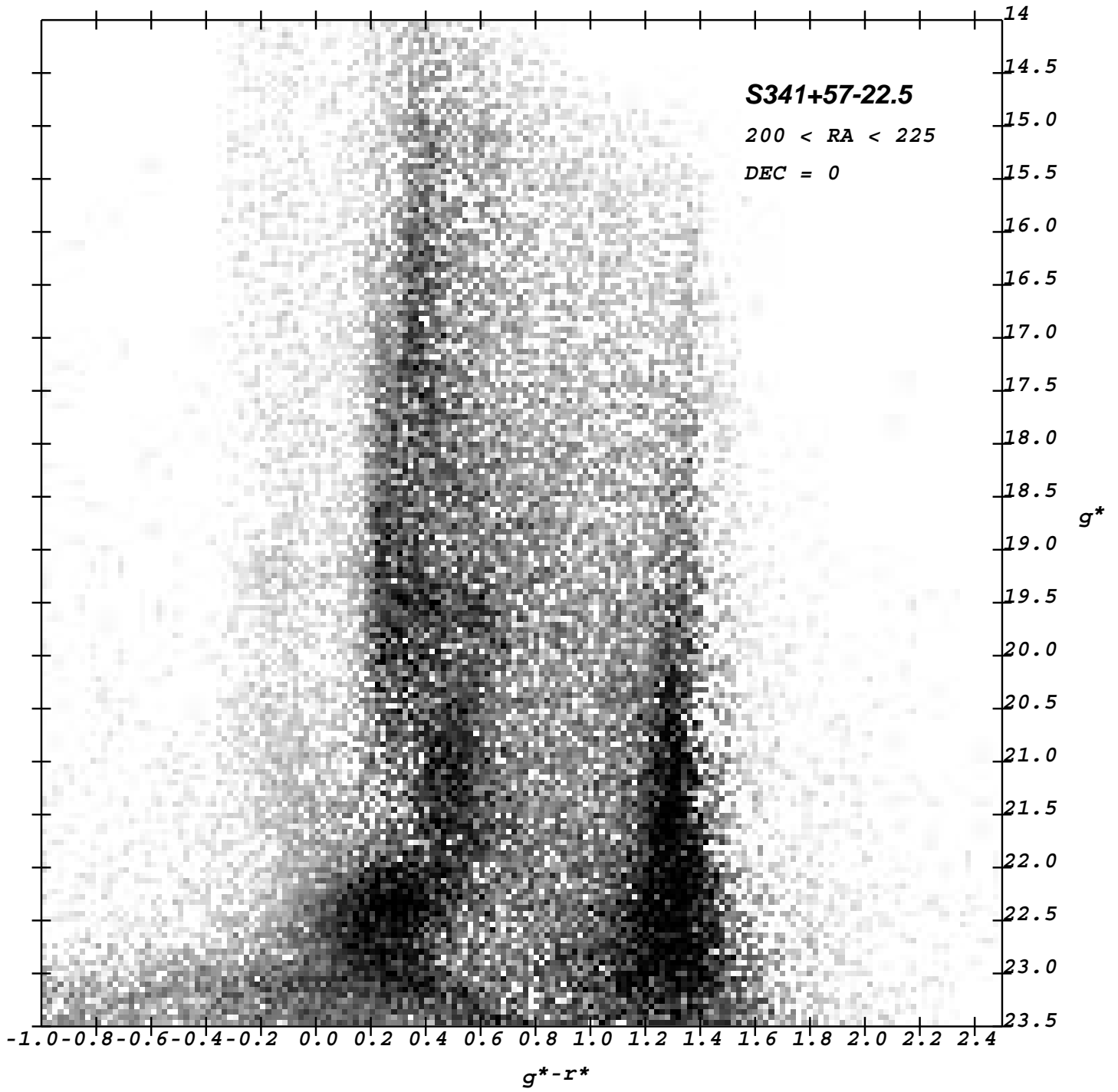
Name	Stripe	Mu	Start RA	End RA	Turnoff	Thick Disk Turnoff
$Sl \pm b - g'$	$^{\circ}$	$^{\circ}$	$^{\circ}$	$^{\circ}$	$g^* - r^*$	$g^* - r^*$
S6+41–20.0	10	235	230	240	0.30	0.40
S167–54–21.5	82	37	0	30	0.22	0.40
S297+63–20.0	10	190	180	200	0.26	0.40
8200–24–19.8	82	75	65	80	0.25	0.32
S223+20–19.4	10	125	117	130	0.28	0.38
S183+22–19.4	37	135	112	125	0.28	0.39
S52–32–20.4	82	320	318	330	0.26	0.40
S218+22–19.5	12	125	125	135	0.28	0.39
S341+57–22.5	10	213	200	226	—	—

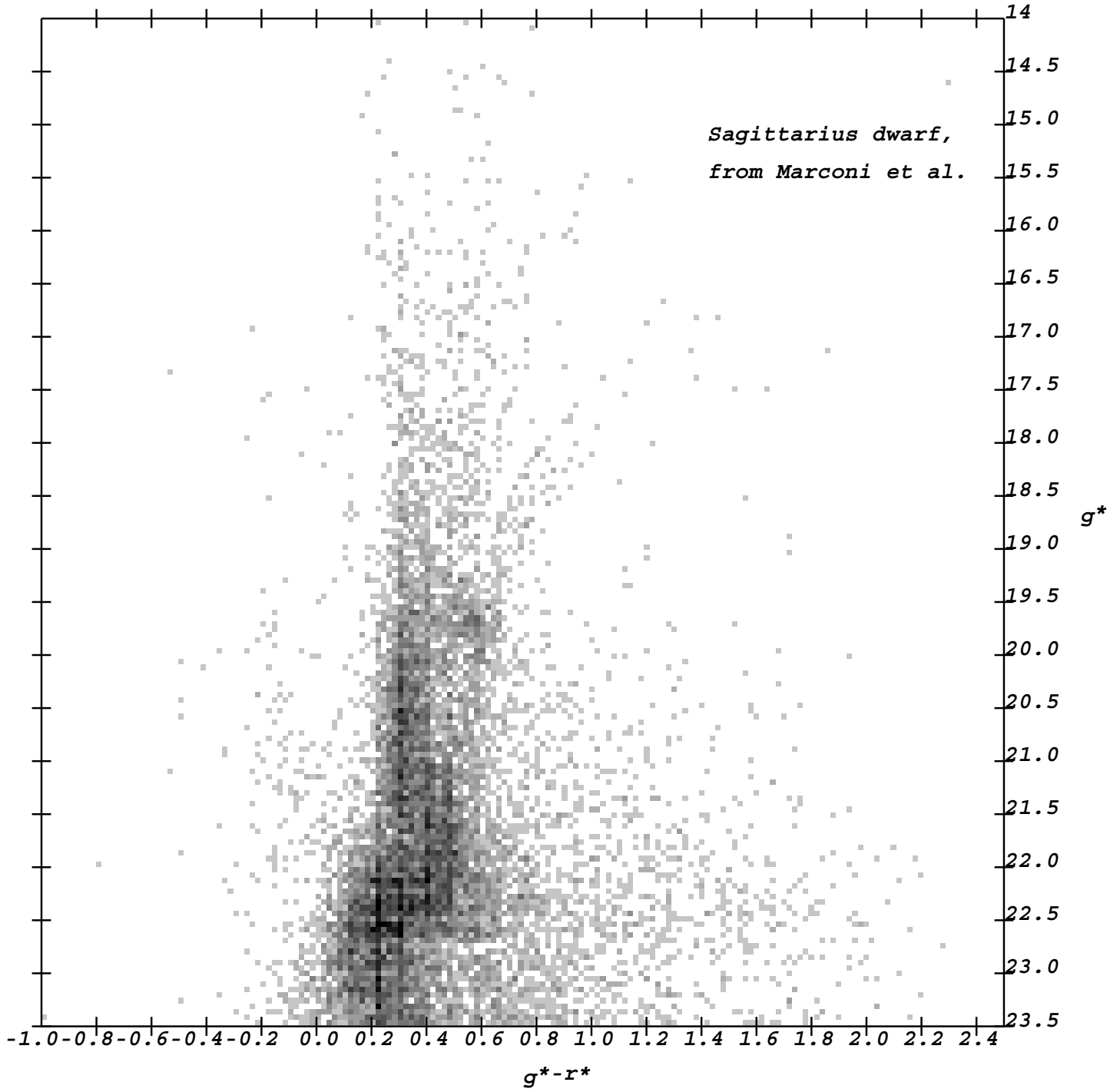


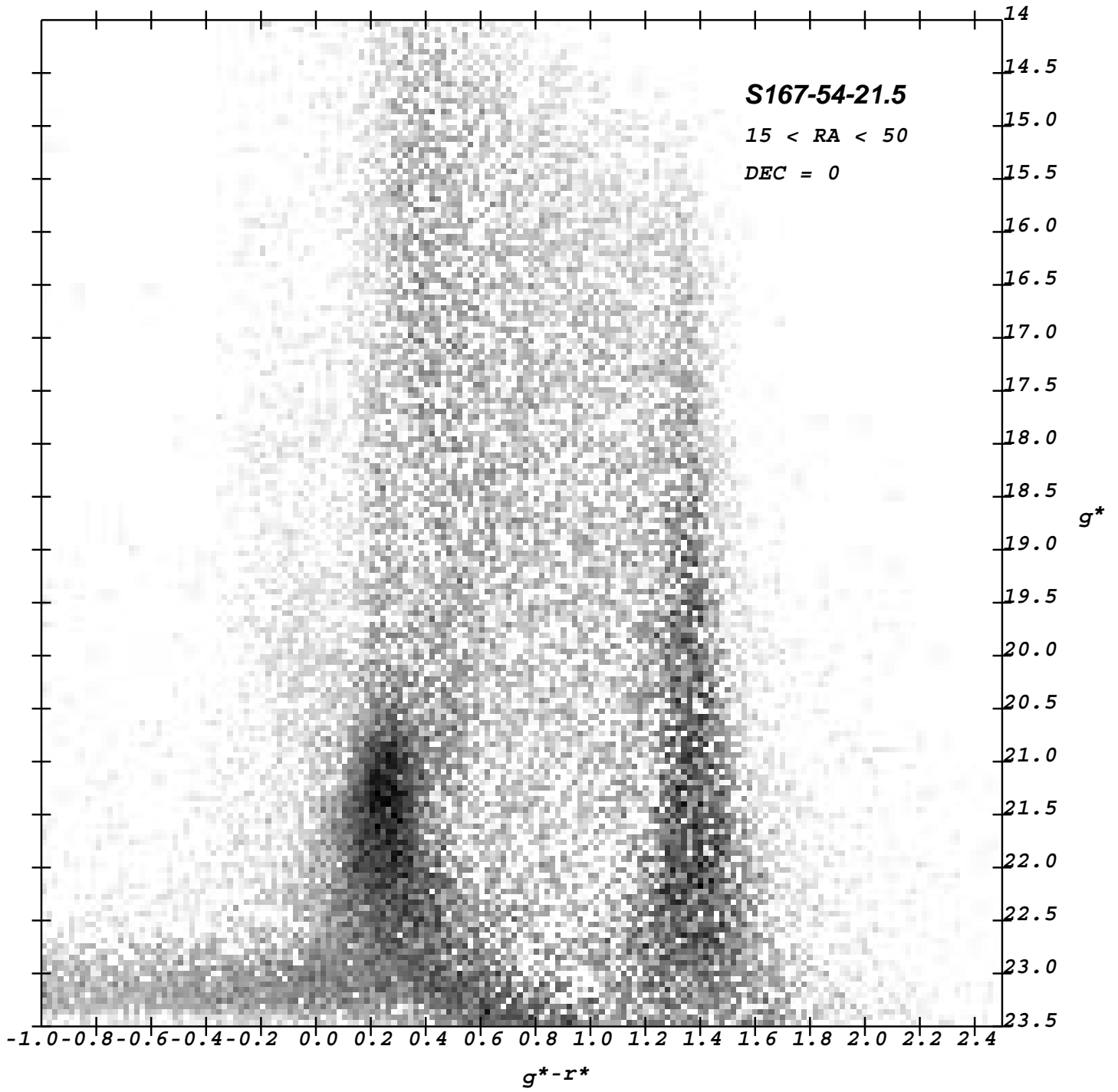


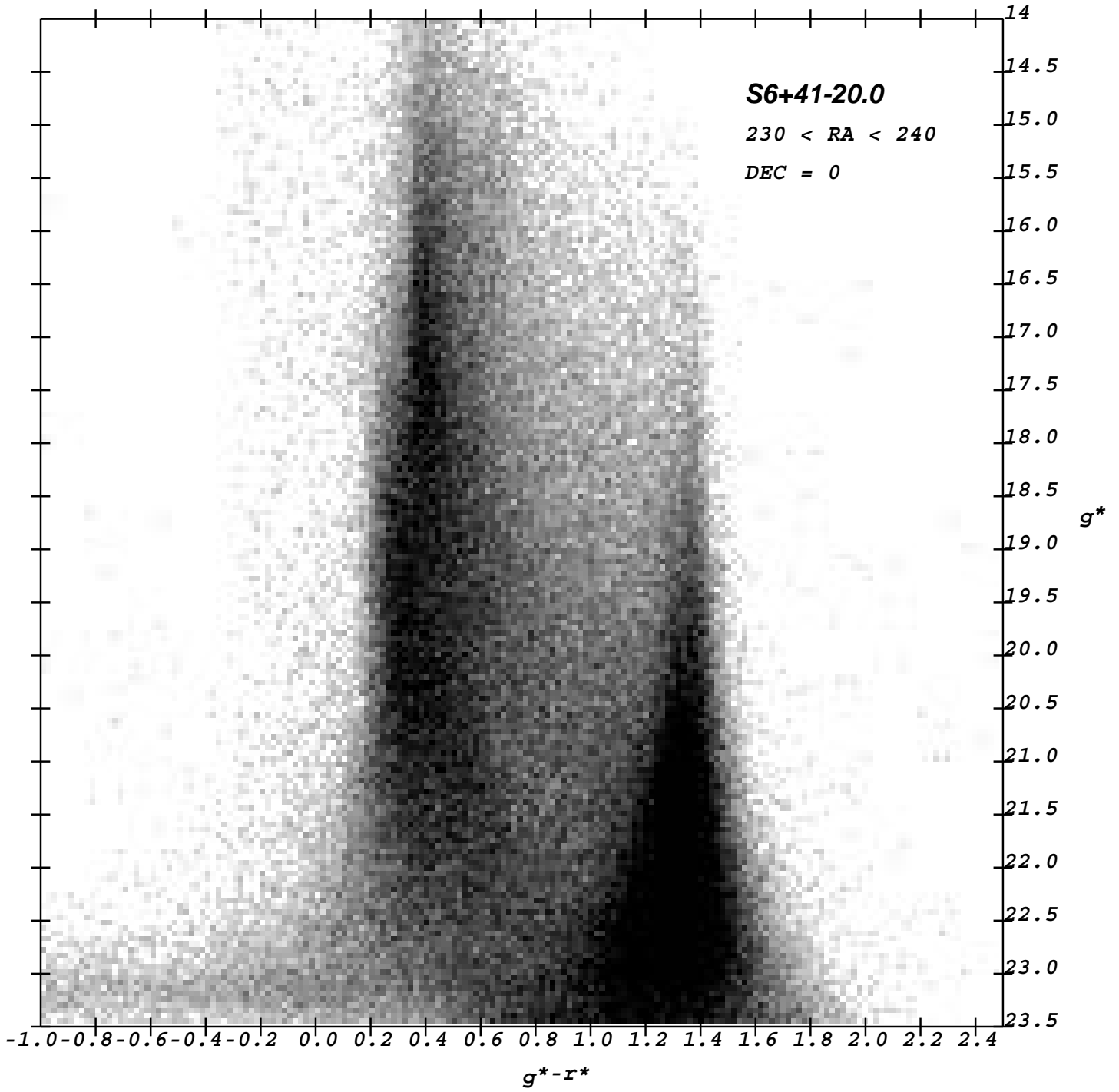


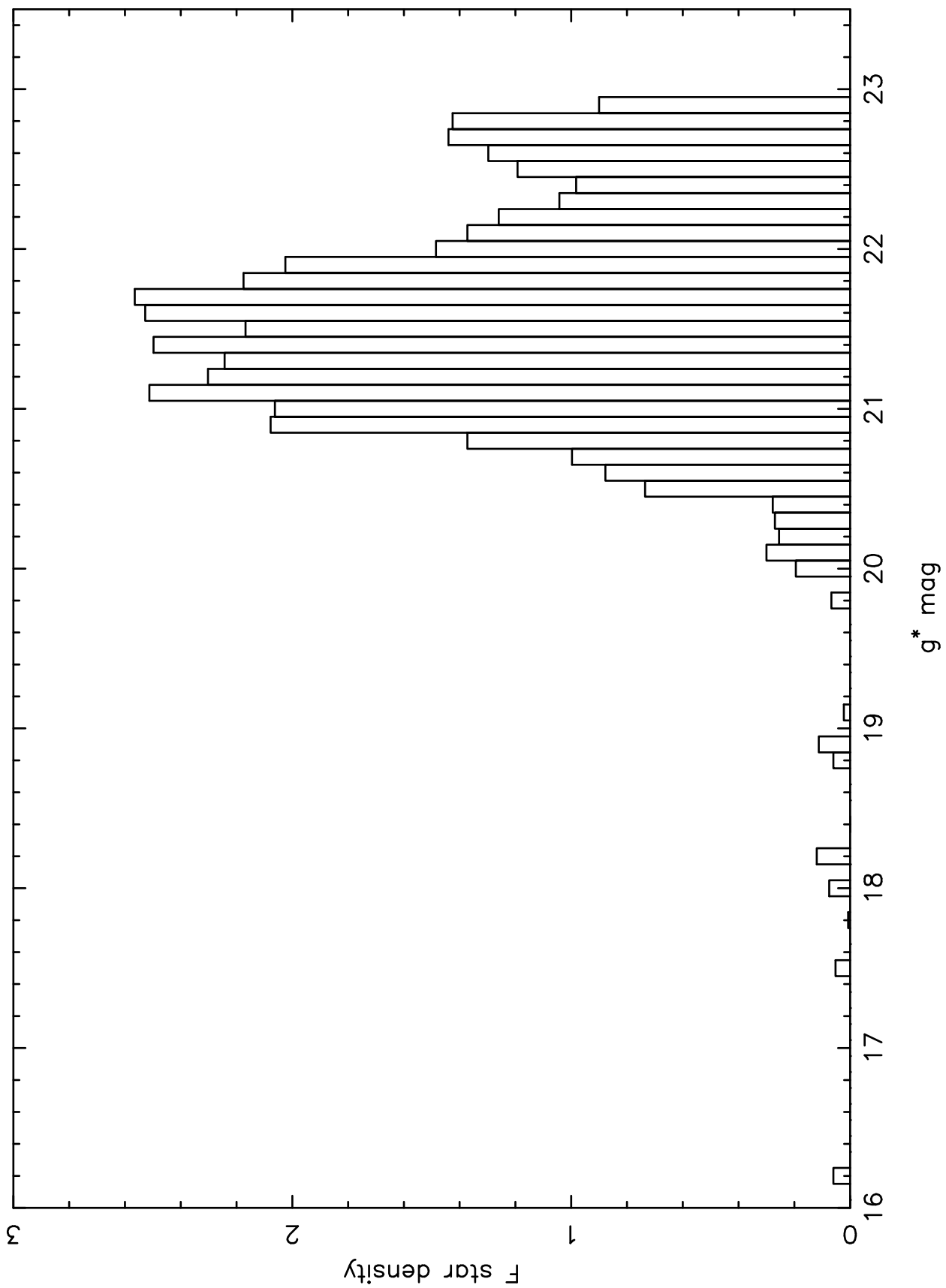




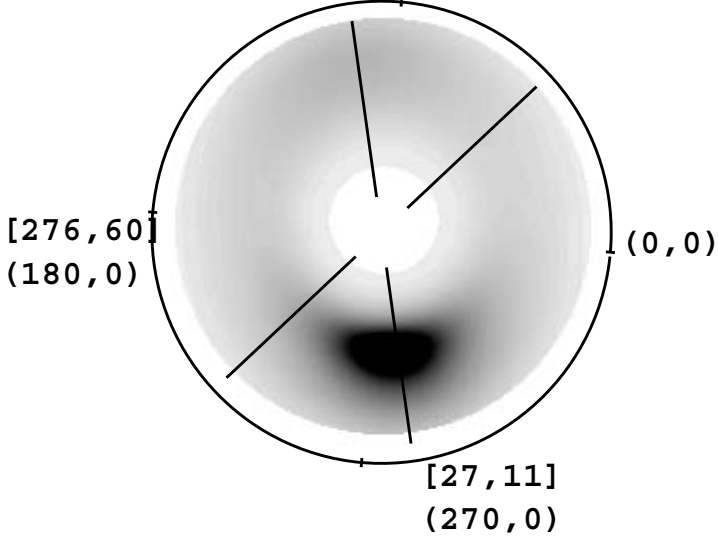




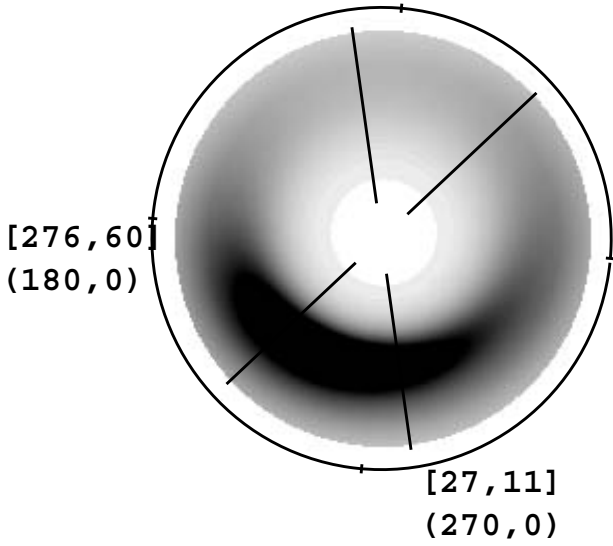
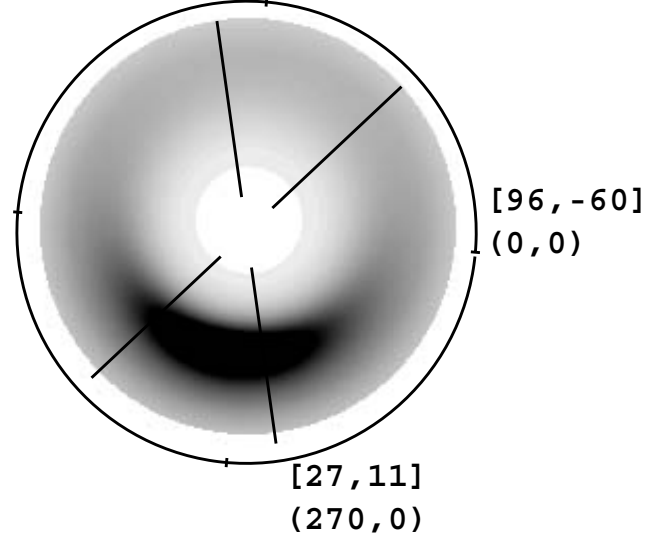




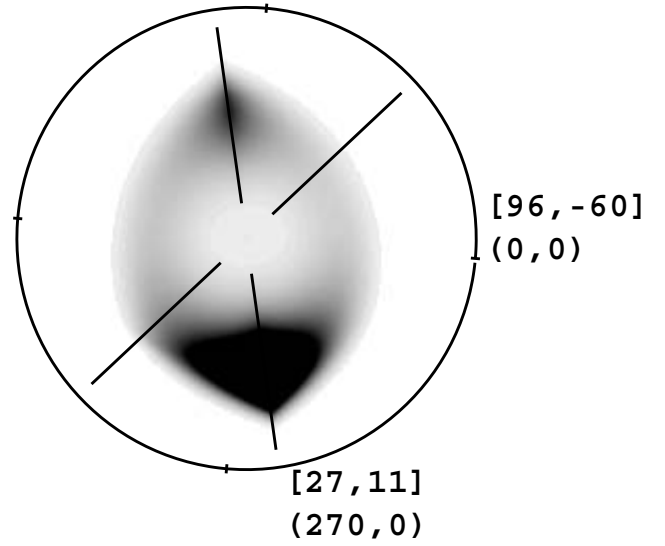
a) $q=0.5$ $\alpha=-3.5$
[207, -11]
(90, 0)



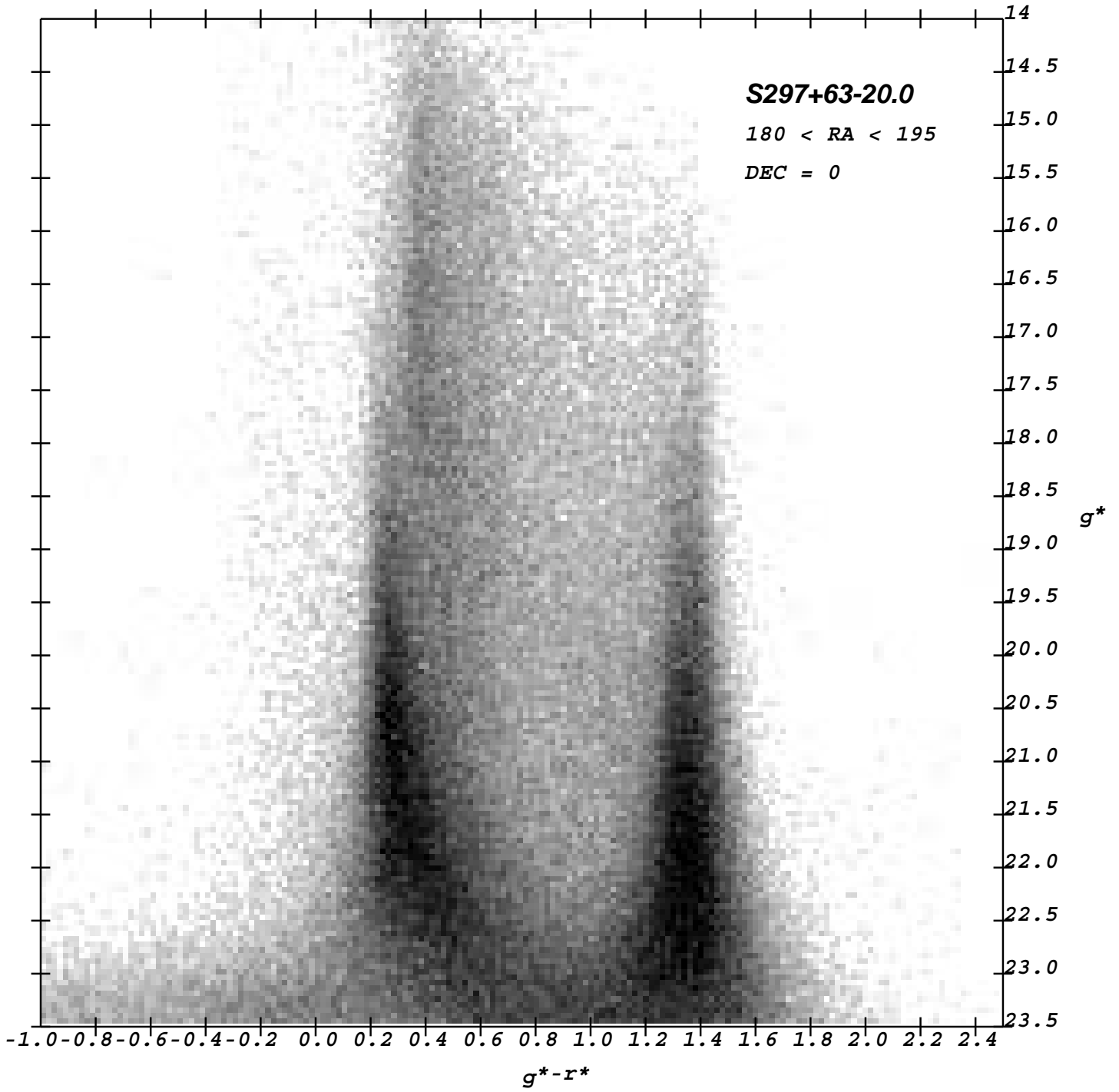
b) $q=1.0$ $\alpha=-3.5$
[207, -11]
(90, 0)

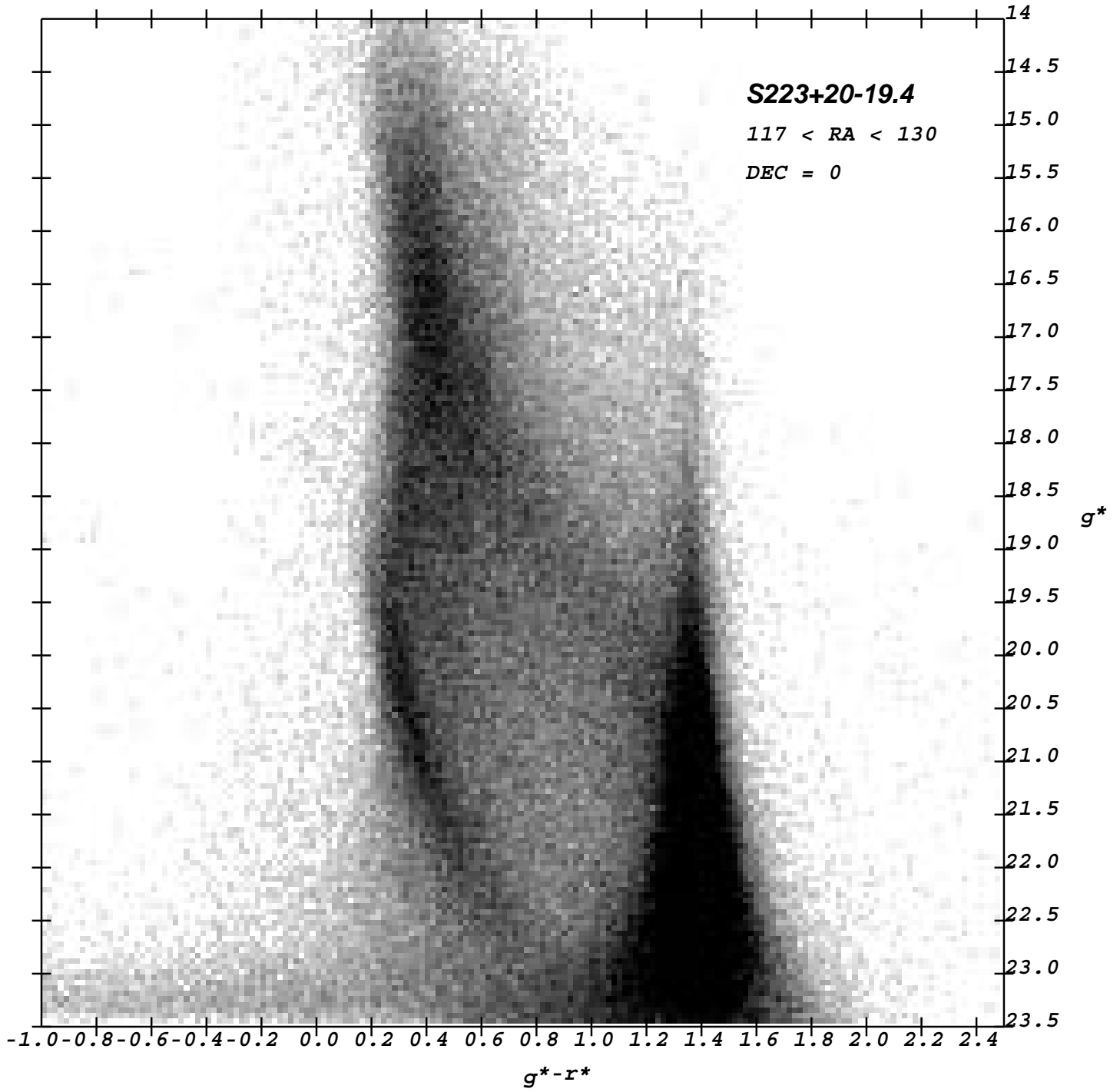


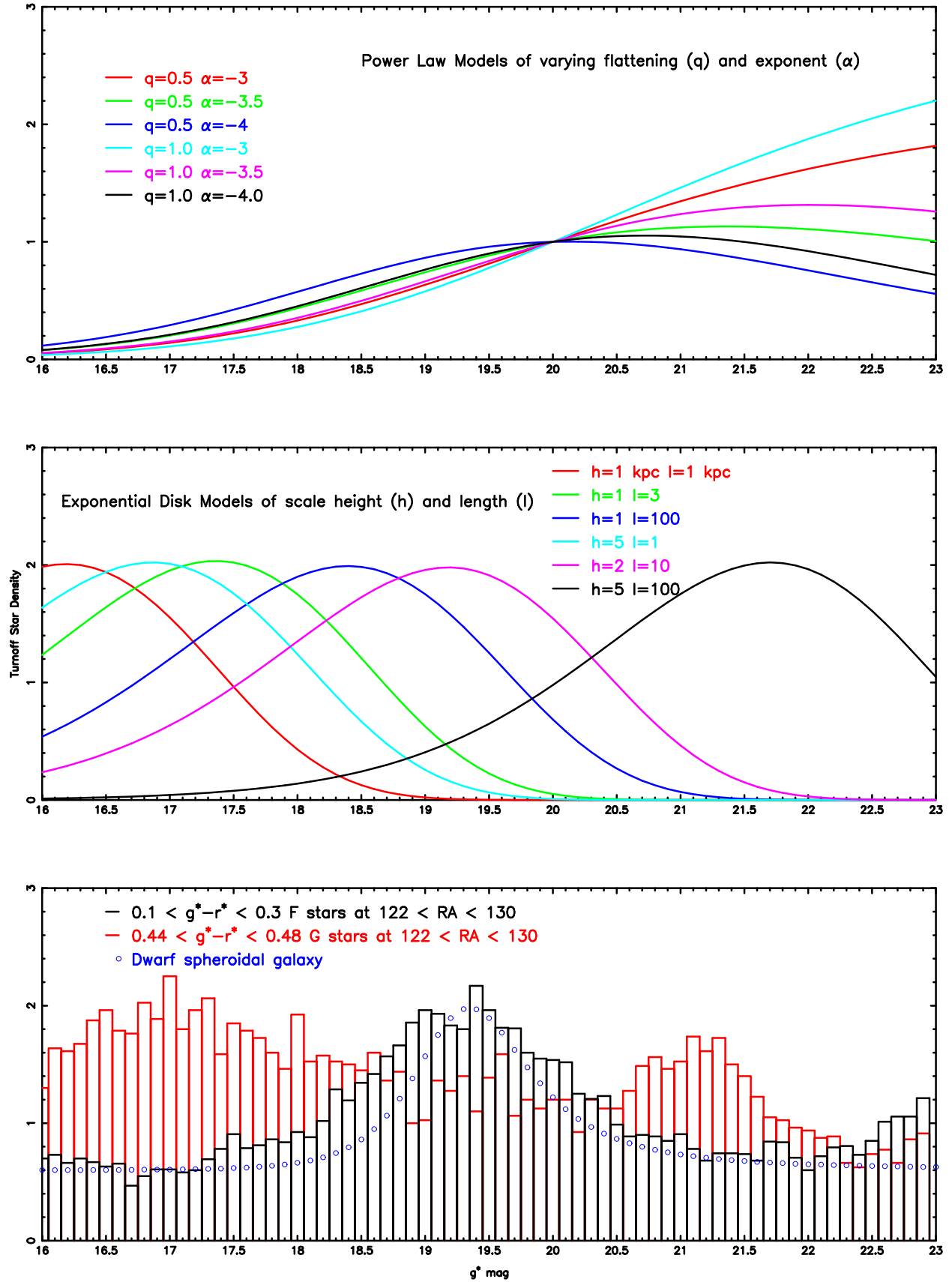
c) $q=1.5$ $\alpha=-3.5$

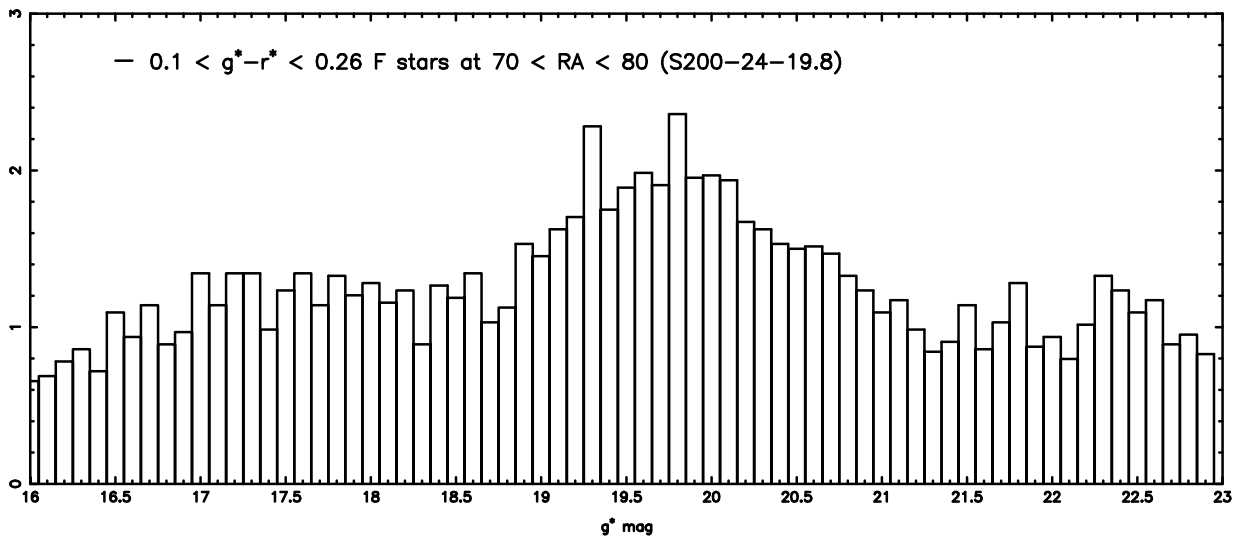
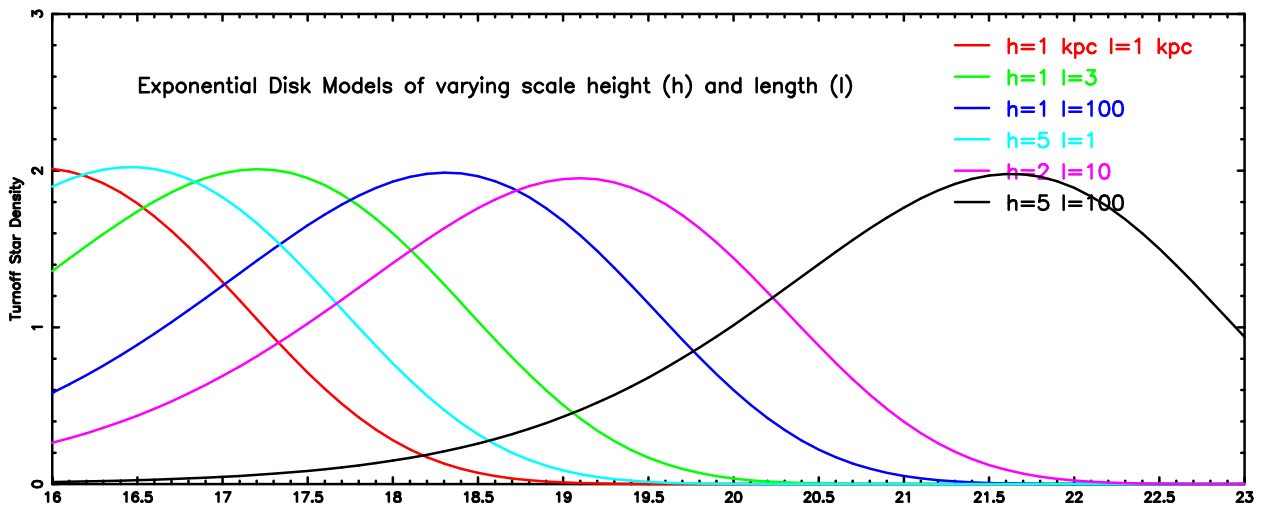
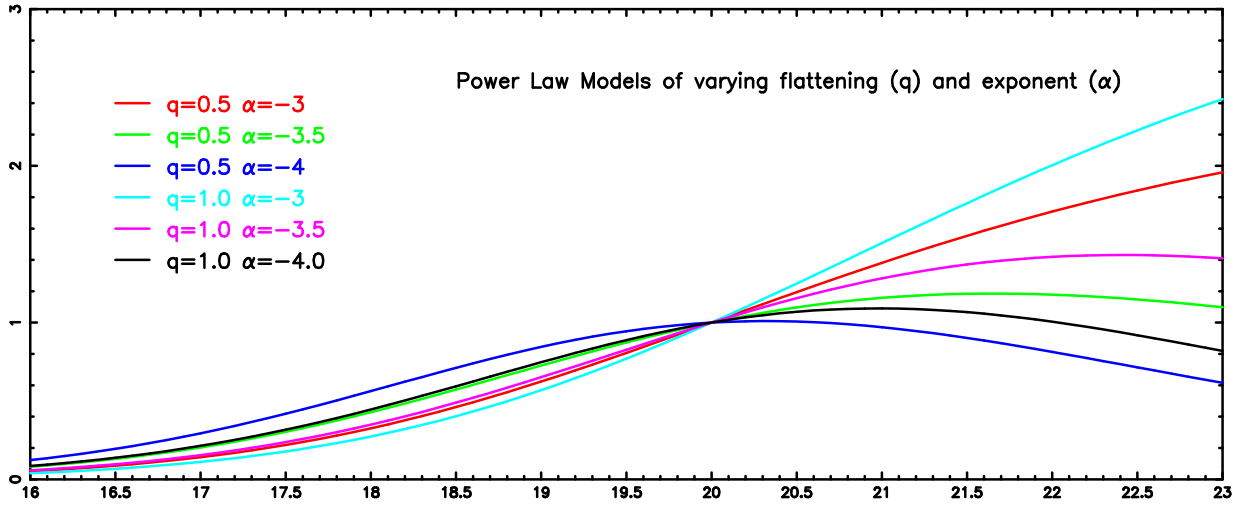


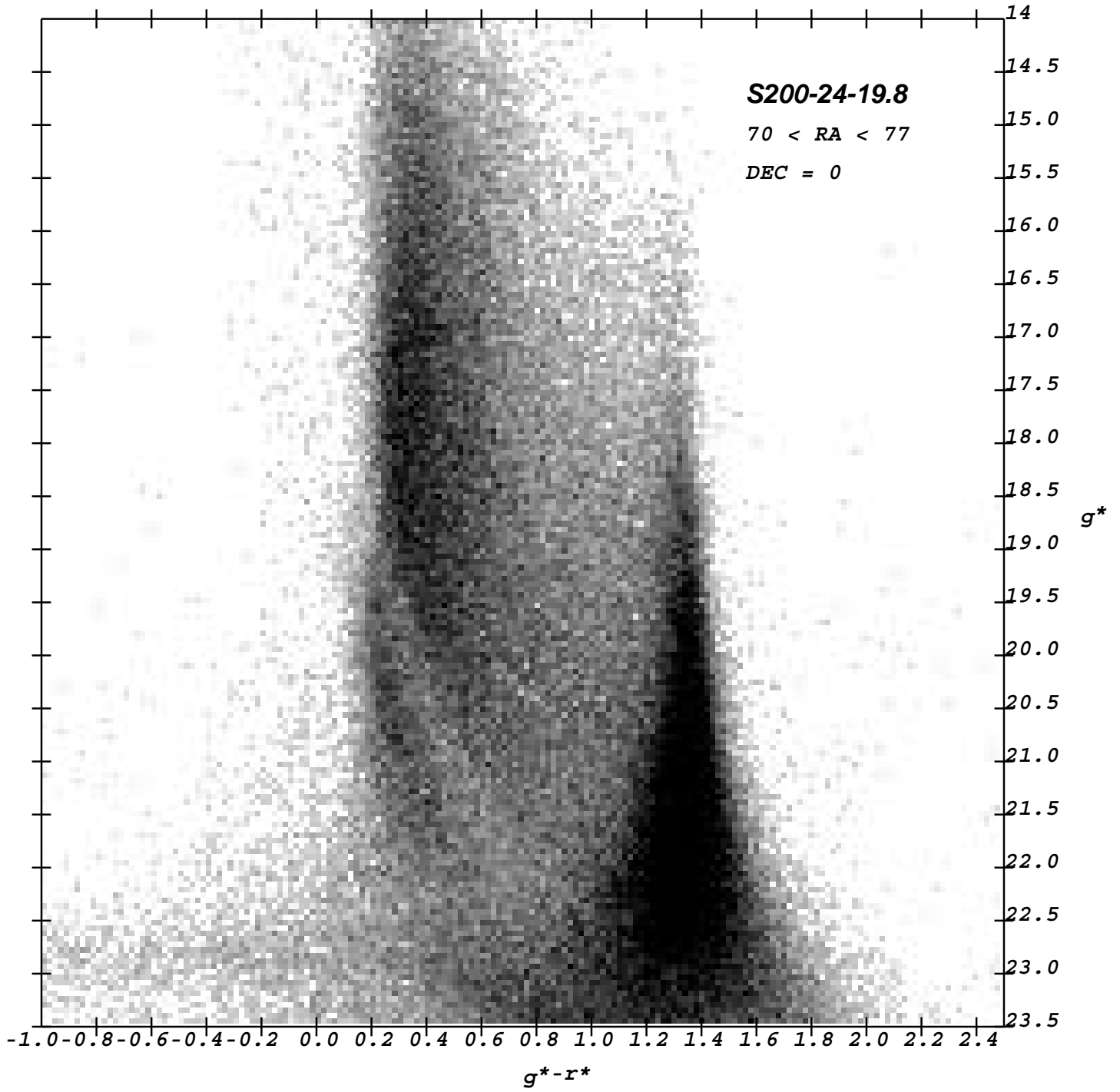
d) $h=1.0$ $l=3.0$ kpc



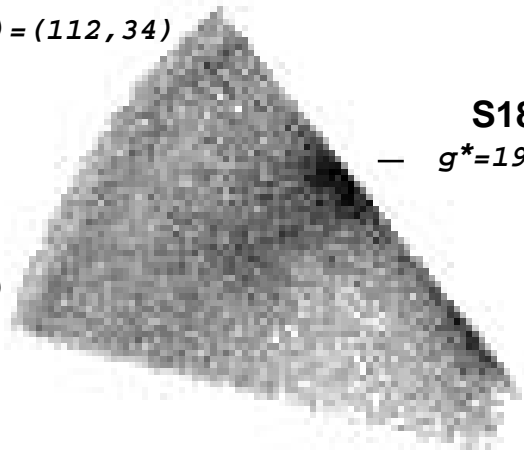








(RA, DEC) = (112, 34)



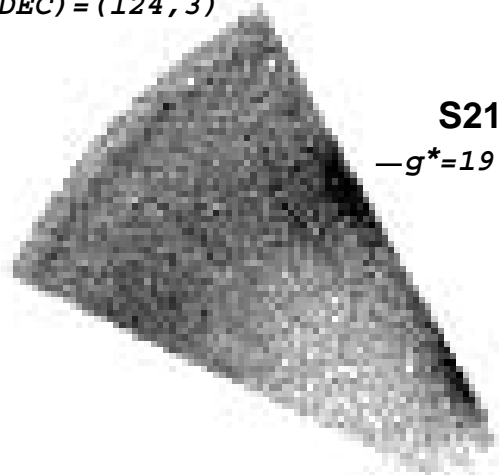
S183+22-19.4

— $g^*=19.4$ (l, b) = (183, 22)

(RA, DEC) = (125, 50)

Stripe 37 $0.1 < g^*-r^* < 0.3$

(RA, DEC) = (124, 3)



S218+22-19.5

— $g^*=19.5$ (l, b) = (218, 22)

(RA, DEC) = (142, 4)

Stripe 12 $0.1 < g^*-r^* < 0.3$

